Master Thesis

Surface plasmon in hollow metallic cylinder

Tian Yuan

Department of Physics, Graduate School of Science
Tohoku University

July 2020

Acknowledgments

In this acknowledgment, I would like to thank everyone who has supported me in finishing my master course and this thesis. First, I would like to express my gratitude to Saito-sensei for his help and guidance not only on finishing my master course. He taught me not only how to conduct physics researches, but also how to present my ideas and communicate with other researchers, which is very important for doing researches in modern days. I also want to express my thankfulness to my families, especially my father, who supported me since I was very young. I would also like to express my special gratitude towards Shofie-san, who have helped me so much as good listener and teacher, and help me a lot at my research. For all of my lab mates : Nuguhara-san, Nguyen-san, Pratama-san, Shirakura-san, Iwasaki-san, Islam-san, Maruoka-san, Wang-san, Pang-san, Maeda-san, It has been a great time to work with you all.

The last but not the least, I would like to address my thankfulness to Tohoku University and IGPAS program for giving me the chance to study and to do research in Japan. This has been my unforgettable experience and I am so lucky to have it.

I also acknowledge the support of GP-Spin program at Tohoku University, without which support this research cannot be finished.

Contents

Chapter 1

Introduction

1.1 Purpose of the study

Enhancement of electromagnetic (EM) field around a metallic nanocylinder is a phenomenon used in a lot of applications, since a metallic nano cylinder with or without a hollow core represents a tip used in tip-enhanced Raman spectroscopy (TERS) [1, 2, 3, 4] and a probe used in scanning nearfield optical microscopy (SNOM) [5, 6]. On the surface of the tip, a strong enhancement of the EM field occurs by surface plasmon (SP), which enhances the signal of TERS and SNOM. Furthermore, since the enhancement occurs at the scale of nanometer, the spatial resolution improves much compared with the wavelength of light. The enhancement around the metallic nanotube also has a potential application for increasing the efficiency of photovoltaic cell [7]. Thus designing a nano-structure with a strong enhancement of the EM field can also help to increase optical absorption or to generate a heat on sample, which is the purpose of this thesis.

The experimental and theoretical researches have shown that the strong enhancement in a metallic cylinder could come from an elementary excitation referred as a SP, which is a collective oscillation of charge density on the surface. The existence and properties of SP on metallic nanocylinder have been studied extensively [8, 1, 9], and it is already been observed in the experiments that SP in nanocylinder is excited by infra-red light. However, even though the existence of SP in a metallic nanocylinder is already studied and well proved, designing the cylinder which gives a strong en-

hancement is not easy as a function of the frequency or the diameter of the core, since that we have no analytical expression of the enhancement. If the relationship between the enhancement of the electric field and the frequency for a given geometry of the light is available, we could synthesize cylinders that gives the best enhancement for a given frequency of the light. In this thesis, we focus on a hollow nano cylinder with a hollow core. The purpose of this work is to analyze the properties of SPs on the nano cylindrical structures, especially the enhancement of electric field in the hollow core caused by SPs, and to represent such enhancement as a function of the geometrical parameters of the cylinder and the frequency of the incident light. In the present thesis, we solve the Helmholtz equation for a EM wave around the cylinder by using several boundary conditions. By solving the equations, we could get the enhancement numerically as a function of the geometrical parameters and incident light frequency, from which we can fit the enhancement to a single function. Such fitted result would be compared with the dispersion of SP.

This master thesis is organized as follows. In the remaining part of Chapter 1 we introduces the background for the present research to help understanding the thesis. In Chapter 2, we discuss the method to calculate the enhancement of EM field in cylindrical system and the calculated energy dispersion of different types of SPs. In Chapter 3, we analyse the enhancement of EM wave by changing the geometrical parameters of the system. In Chapter 4, we will discuss the fitted analytical expressions of the enhancement, absorption probability and other properties of the enhancement. In Chapter 5, we give conclusion of the thesis.

1.2 Background

Here we show some basic concepts which are important for understanding this thesis.

1.2.1 Plasmon and surface plasmon oscillation

Plasma refers to a state of material, in which the positive and negative charges in the material are unbounded or weakly bounded by the Coloumb interaction to each other and delocalized. In the metals, since the electrons can move in a background of positive ions, an electron plasma can be excited. A plasmon is an elementary excitation of the

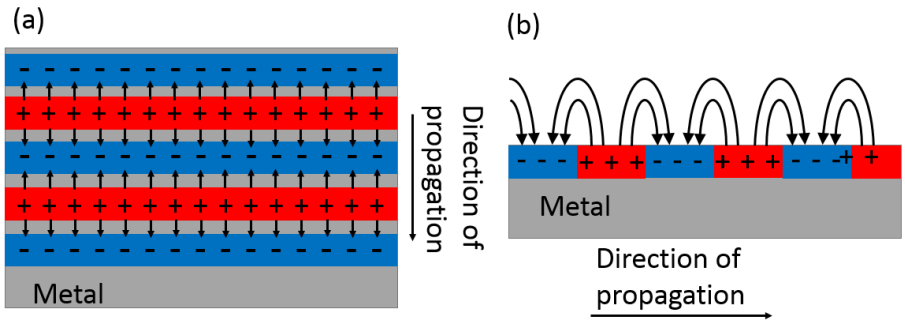

Figure 1.1 (a) Illustration of the bulk plasmon, electrons oscillate away from its original position, creating a longitudinal polarization field. (b) Illustration of the surface plasmon, charge density oscillation occurs on the surface, creating an polarization that is transversal to propagation direction. Arrowed lines in the figures are the electric field line.

plasma. In the case of metal, a plasmon is a propagating wave of the oscillation of the electron density in the positive background. There are two types of the plasmons, a bulk plasmon and a surface plasmon (SP), which are shown in Fig. 1.1

For bulk plasmon, electrons are oscillating in the direction parallel to the propagation direction of the wave. Such plasmon creates a longitudinal displacement to electric field and propagates inside the material. The bulk plasmon is observed by the electron energy loss spectroscopy (EELS) [10, 11]. The bulk plasmon, being a longitudinal wave, can not be excited directly by the light since the light is a transverse wave. In the case of SP, the charge density oscillates at the surface of the material, creating a transverse displacement, which resembles a light. It is already well known that the surface plasmon can be excited by light [9, 12]. SP is also defined as a light that is confined on the boundary of materials [13]. In theory, a SP can only exist on the interface between a material with positive permittivity (dielectric material for example) and a material with negative permittivity that can support free charges (metals for example) [14].

Despite the fact that SPs can be treated as quasi-particles with mass and energy [?, 15], in practice, SPs are often described with classical electromagnetism. Studies conducted on surface plasmon using classical methods have been proven satisfying enough in covering most of the important properties of SPs. It is argued in some of the previous studies that many quantum behaviors of the SPs are already described

Fig. 1.1: Fig/plasmon.png

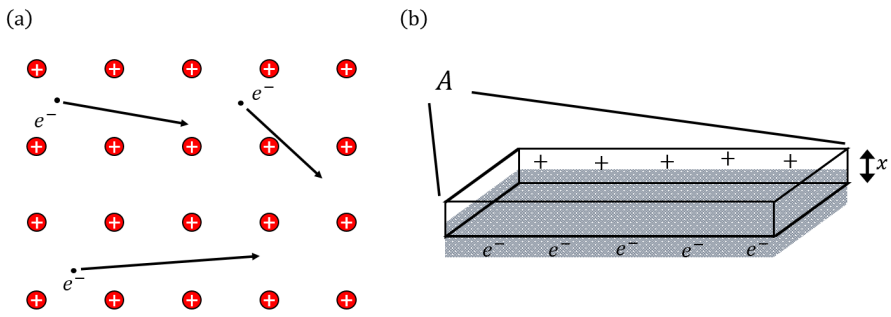

Figure 1.2 (a) The schematic of the Drude model, electrons moves freely in a background of positive ions. (b) The electrons are displaced with a distance x with respect to the background, in a volume with the cross section A.

within the dielectric function describing metal permittivity [10, 12, 16].

1.2.2 The Drude model

Since SP is a quantum of collective motion of electrons, it is important for us to describe an electron in a metal. The Drude model or free electron model is a classical model for describing the behavior of electron. In this model, the electron is treated as a free particle that moves in a background of positive ionic cores, as is shown in Fig. 1.2 (a). Equation of motion of the electron in the electric field is given by,

$$m\frac{\mathrm{d}^2[\mathbf{r}(t)]}{\mathrm{d}t^2} + \frac{m}{\tau}\frac{\mathrm{d}[\mathbf{r}(t)]}{\mathrm{d}t} = -e\mathbf{E}(t), \tag{1.1}$$

where m denotes the mass of the electron, $\mathbf{r}(t)$ is the position of the electron, τ is a relaxation time, which means an average time of a electron to lose the kinetic energy, e stands for the elementary charge and $\mathbf{E}(t)$ is a time-dependent external electric field [12]. Let us consider the harmonic time-dependence for $\mathbf{E}(t)$ and $\mathbf{r}(t)$ given as follows:

$$\mathbf{E}(t) = \mathbf{E_0}e^{-i\omega t}, \tag{1.2}$$

$$\mathbf{r}(t) = \mathbf{r_0}e^{-i\omega t}. \tag{1.3}$$

Fig. 1.2: Fig/drudedielec.png

By substituting Eqs. (1.2) and (1.3) into Eq. (1.1), we can get the following equations.

$$-m\omega^2\mathbf{r}(t) - \frac{im}{\tau}\omega\mathbf{r}(t) = -e\mathbf{E}(t),$$
$$\mathbf{r}(t) = \frac{e\mathbf{E}(t)}{m\omega^2 + im/\tau}. \tag{1.4}$$

By setting $\gamma = 1/\tau$ as the damping rate, an induced electric polarization is given by $\mathbf{r}(t)$ as follows:

$$\mathbf{P}_e(t) = -ne\mathbf{r}(t) = -\frac{ne^2}{m\omega^2 + i\gamma\omega}\mathbf{E}(t), \tag{1.5}$$

where n refers to the number density of electrons. By adding Eqs. (1.5) with the polarization of the background $\mathbf{P}_b$, we obtain the total polarization of a metal as follows [17]:

$$\mathbf{P}(t) = \mathbf{P}_b(t) + \mathbf{P}_e(t) = \left(\chi_b - \frac{ne^2}{m\omega^2 + im\gamma\omega}\right)\mathbf{E}(t), \tag{1.6}$$

where χ_b is the background polarizability. The electric displacement vector in the metal is given by

$$\mathbf{D}(t) = \varepsilon_r\varepsilon_0\mathbf{E}(t) = \varepsilon_0\mathbf{E}(t) + \mathbf{P}(t)$$
$$= \varepsilon_0\left[1 + \chi_b/\varepsilon_0 - \frac{ne^2}{m\varepsilon_0(\omega^2 + i\gamma\omega)}\right]\mathbf{E}(t). \tag{1.7}$$

By defining the relative permittivity of the background as: $\varepsilon_b = 1 + \chi_b/\varepsilon_0$, we get the relative permittivity of metal ε_r from the Drude model as follows:

$$\varepsilon_r(\omega) = \varepsilon_b - \frac{\omega_p^2}{\omega^2 + i\gamma\omega}, \tag{1.8}$$

where we define the bulk plasmon frequency ω_p as follows:

$$\omega_p = \sqrt{\frac{ne^2}{m\varepsilon_0}}. \tag{1.9}$$

To understand the physical meaning of ω_p, we will now derive the bulk plasmon frequency ω_p of a metal by considering the situation where free electrons in a volume of space with cross sectional area A has been displaced with distance r, as is shown in Fig. 1.2 (b). From the Gauss law, we can get the electric field caused by such displacement as follows:

$$E = \frac{Q}{A\varepsilon_0} = \frac{neAr}{A\varepsilon_0}$$
$$= \frac{ner}{\varepsilon_0}. \tag{1.10}$$

By substituting Eq. (1.10) into Eq. (1.1) and assuming that there is no collision of electrons i.e. $1/\tau = \gamma = 0$, we get

$$\begin{aligned} nm\frac{\mathrm{d}^2 r}{\mathrm{d}t^2} &= -neE \\ &= -\frac{n^2 e^2 r}{\varepsilon_0} \iff \frac{\mathrm{d}^2 r}{\mathrm{d}t^2} + \frac{ne^2}{m\varepsilon_0} r = 0. \end{aligned} \tag{1.11}$$

Eq. (1.11) describes the motion of free electron gas under a self-sustaining electric field, which is an equation of motion of an harmonic oscillator. This equation describes an intrinsic oscillation of electrons in metal, whose frequency is the bulk plasmon frequency $\omega_p = \sqrt{\frac{ne^2}{m\varepsilon_0}}$ [12].

We find that the permittivity in Eqs. (1.9) is a function of incident light frquency ω. It is noted that ω_p is only related to the electron density n. On the other hand γ is related to the Fermi velocity v_F and electron mean free path l as: $\gamma = 1/\tau = v_F/l$. For an ideal metal, the permittivity is calculated as a function of n, l, v_F and ε_b. However, actual metals under common circumstances and optical frequencies are not ideal conductors. Effective parameters fitted from data gatherd in experiment is used in actual study [18, 19, 1]. With the electric permittivity derived, we are ready to start the mathematical description of SPs starting from the classical electromagnetism. The description of SPs using the classical electromagnetism is appropriate when the size of the material is larger than 10 nm. Otherwise the quantum description should be used. For the calculations in this thesis, we are going to focus on the phenomena happening on gold structures. The parameters were taken: $\varepsilon_b = 5.9673$, $\omega_d/(2\pi) = 2113.6$ THz, $\gamma = 15.92$ THz [20].

1.2.3 Surface plasmon and near field enhancement

Next we want to introduce some applications, excitation and observation of SPs in experiments, then we will present a simple numerical descriptions of a certain type of SPs.

The SP is a well observed phenomenon that has been used for a wide range of applications. The earliest phenomenon observed which is later proven to be related to the SPs, is color-stained glass due to the absorption of the light caused by localized SP resonance on noble metal particles [12]. Such technique of color-staining was fist used in fourth century Europe but without a good physical explanation until the theory of

plasmonics was developed. It is understood now that such coloring is caused by the optical absorption due to the excitation of SPs. Beside staining the glass, local field enhancement and optical absorption by localized SP resonance on metallic particles also find more modern applications in photovoltaic devices [12, 9], bio science/medical detection [21] and spectroscopies [22]. Such localized SPs can also be found on a cylinder when SPs oscillate around the circumference of the cylinder [23, 24].

As has been proven in experiments, localized SPs can be excited by directly shading light on a metallic sphere or a cylinder. The excitation induces a strong near field enhancement, as is shown in Fig. 1.3 (a) and (b). This is one of the easiest ways to excite SPs, with many detailed researches and experiments conducted to observe and utilize the near field enhancement. It is noted that besides a localized SP, a cylinder can also support a SP that propagates in axial direction, as is shown in Fig. 1.3 (c). In most of actual experiments, both the localized and the propagating SPs are excited [25, 26]. The near field enhancement around the cylinder could find similar uses as that around sphere, such as enhancing the EM field intensity, increasing the absorption of the light and increasing signal intensity in spectroscopies. SPs propagating along axial direction of a cylinder can be excited by an incident light in one tip of the cylinder and emit the light on the other tip, which is capable of carrying the information along the axis of the cylinder [27].

The most mathematically intuitive case of a SP is a propagating SP on a flat surface. In the following discussion we want to provide a simple analysis of SP on a flat surface to serve as a simple example for understanding more mathematically complicated cases of SPs on a cylinder. By solving the Maxwell equations on a flat surface, we will get two groups of equation, each group defines a solution of a specific surface wave mode. More specifically, by assuming that the surface wave mode propagates in the x-direction with wave vector k_x, we can get the EM fields of the surface modes as is shown in Fig. 1.4.

Let us start with one of solution of the surface mode, which is shown in Fig. 1.4 (a). The mode has in-plane magnetic field that is transverse to propagation direction, hence such mode was refereed as a transverse magnetic (TM) mode. The expressions

Fig. 1.3: Fig/samples.png
Fig. 1.4: Fig/flat-sp.PNG

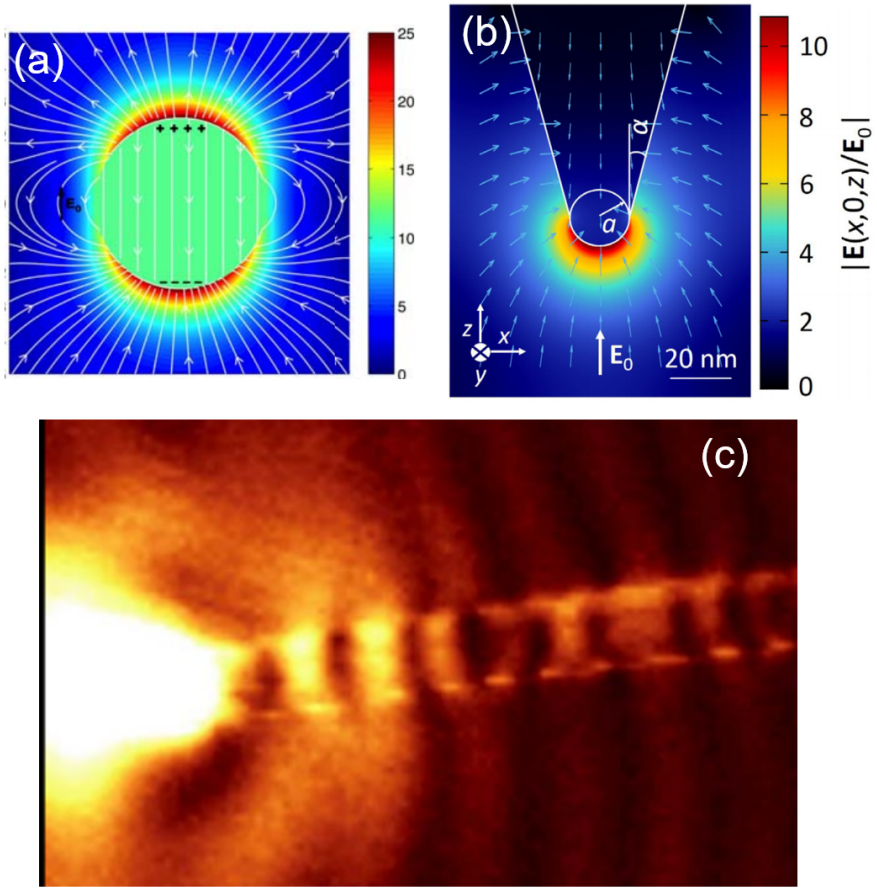

Figure 1.3 (a) The enhancement caused by localized surface plasmon around a gold sphere [28]. (b) Near field enhancement around the head of a probe used in TERS. The tip is comparable to a metallic cylinder [1]. (c) EM field dispersion of SPs in a silver nanowire [29].

of the EM fields of TM mode are given by

$$
\begin{aligned}
H_y^{(1)} &= a_1 e^{ik_x x} e^{\kappa_{z1} z}, \\
E_x^{(1)} &= -i a_1 \frac{\kappa_{z1}}{\omega \varepsilon_1 \varepsilon_0} e^{ik_x x} e^{\kappa_{z1} z}, \\
E_z^{(1)} &= -a_1 \frac{k_x}{\omega \varepsilon_1 \varepsilon_0} e^{ik_x x} e^{\kappa_{z1} z},
\end{aligned} \tag{1.12}
$$

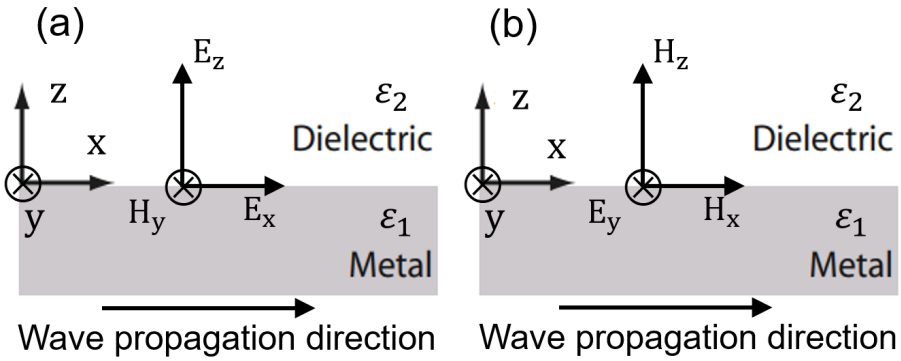

Figure 1.4 Schematic of surface modes on a metallic flat surface in a dielectric background, relative permittivity(permeability) of the metallic part and the dielectric part is ε_1 (μ_1) and $\varepsilon_2(\mu_2)$, respectively. (a) A surface TM mode, containing a transverse electric field. (b) A surface TE mode, containing a transverse magnetic field.

and

$$\begin{aligned} H_y^{(2)} &= a_2 e^{ik_x x} e^{-\kappa_{z2} z}, \\ E_x^{(2)} &= i a_2 \frac{\kappa_{z2}}{\omega \varepsilon_2 \varepsilon_0} e^{ik_x x} e^{-\kappa_{z2} z}, \\ E_z^{(2)} &= -a_2 \frac{k_x}{\omega \varepsilon_2 \varepsilon_0} e^{ik_x x} e^{-\kappa_{z2} z}, \end{aligned} \tag{1.13}$$

where κ_{z1} and κ_{z2} are the decay constants on the z-direction, which are given as follow:

$$\kappa_{z1} = \sqrt{k_x^2 - k_0^2 \mu_1 \varepsilon_1}, \tag{1.14}$$

$$\kappa_{z2} = \sqrt{k_x^2 - k_0^2 \mu_2 \varepsilon_2}, \tag{1.15}$$

with μ_n (ε_n) is the relative permeability (permittivity) of the n-th medium, $k_0 = \omega/c$ is the wavevector of EM wave in the vacuum. $E_i^{(n)}$ and $H_i^{(n)}$ in Eqs. (1.12) and (1.13) denote electric and magnetic field intensities on i-th axis in the n-th medium, respectively, and a_n is the amplitude of $H_y^{(n)}$. As is shown in Eqs. (1.12) and (1.13), a TM mode has a component of electric field in the direction of propagation, as is shown in Fig. 1.5 (a), which indicates that there is an displacement of the charge density along the propagation direction, i.e. a propagating plasmon.

Fig. 1.5: Fig/distriflat-sp.PNG

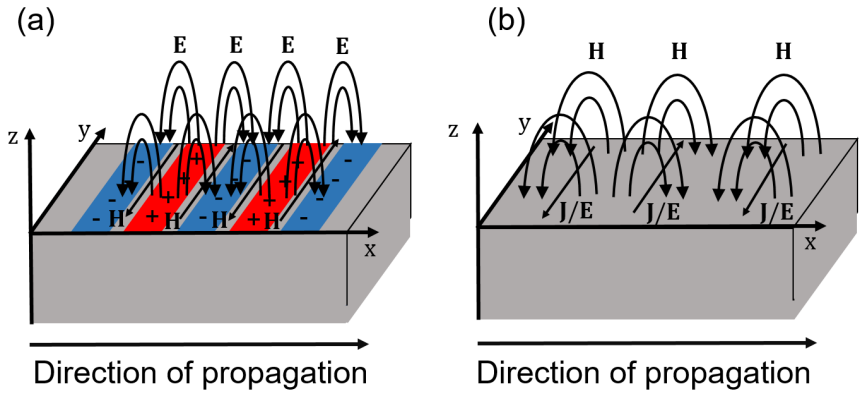

Figure 1.5 (a) A surface TM mode, manifesting an oscillation of surface charge density in the direction of propagation. (b) A surface TE mode, manifesting an oscillation of surface current density (J) perpendicular to that of the propagation direction.

The expressions of EM fields of another group of surface mode are given as follows:

$$\begin{aligned} E_y^{(1)} &= a_1 e^{ik_x x} e^{\kappa_{z1} z}, \\ H_x^{(1)} &= -ia_1 \frac{\kappa_{z1}}{\omega\mu_1\mu_0} e^{ik_x x} e^{\kappa_{z1} z}, \\ H_z^{(1)} &= -a_1 \frac{k_x}{\omega\mu_1\mu_0} e^{ik_x x} e^{\kappa_{z1} z}, \end{aligned} \tag{1.16}$$

and

$$\begin{aligned} E_y^{(2)} &= a_2 e^{ik_x x} e^{-\kappa_{z2} z}, \\ H_x^{(2)} &= ia_2 \frac{\kappa_{z2}}{\omega\mu_2\mu_0} e^{ik_x x} e^{-\kappa_{z2} z}, \\ H_z^{(2)} &= -a_2 \frac{k_x}{\omega\mu_2\mu_0} e^{ik_x x} e^{-\kappa_{z2} z}, \end{aligned} \tag{1.17}$$

where the mode has a component of electric field only in the direction perpendicular to that of the propagation. Hence the mode is known as the transverse electric (TE) mode. Since the electric field is perpendicular to the propagation direction, TE mode is not a surface plasmon. TE mode is composed by an oscillation of surface current density (J), in which the direction of the current density is perpendicular to the direction of the propagation, as is shown in Fig. 1.5 (b).

The dispersion relation of the surface mode determines the resonant condition of the system, as a surface mode will be excited by light only when the incident light has

Fig. 1.6: Fig/disperflat.PNG

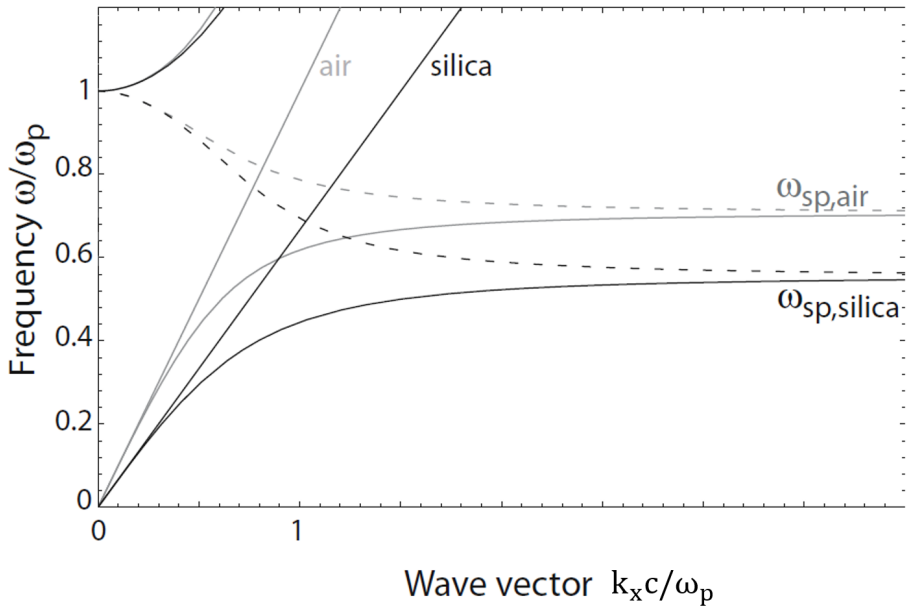

Figure 1.6 Dispersion relation ω_{sp} of surface plasmon on a flat silver/silica boundary and a silver/air boundary, straight line represents the dispersion of the light [12].

a frequency and a component of wavevector parallel to the surface that are equal to those of the SP. The EM fields of surface modes should satisfy the boundary conditions of the EM field, that is, the tangential components of E and H are continuous on the surface. For TE mode, from Eqs. (1.16) and (1.17), we get the following equations at $z = 0$:

$$E_y^{(1)} = E_y^{(2)} \leftrightarrow a_1 = a_2, \tag{1.18}$$

$$H_x^{(1)} = H_x^{(2)} \leftrightarrow a_1 \frac{\kappa_{z1}}{\omega\mu_1\mu_0} = -a_2 \frac{\kappa_{z2}}{\omega\mu_2\mu_0}. \tag{1.19}$$

From which we get the dispersion relation of the TE mode as follows:

$$\kappa_{z1}\mu_2 = -\kappa_{z2}\mu_1. \tag{1.20}$$

By noticing that we are discussing a surface mode, both κ_{z1} and κ_{z2} should have to be positive to ensure a decaying field on the z direction, which means either μ_1 or μ_2 should be negative. Materials with negative permeability is not found in nature, therefore the TE mode is not exited in the normal material. Some experiments had successfully observed surface confined TE modes on a metamaterial [30, 31]. In this thesis however we would not discuss the nature of the TE mode.

For TM mode, from Eqs. 1.12 and Eqs 1.13 and boundary conditions we can get the following equations at $z = 0$:

$$\begin{aligned} H_y^{(1)} = H_y^{(2)} &\leftrightarrow a_1 = a_2, \\ E_x^{(1)} = E_x^{(2)} &\leftrightarrow a_1 \frac{\kappa_{z1}}{\omega\varepsilon_1\varepsilon_0} = -a_2 \frac{\kappa_{z2}}{\omega\varepsilon_2\varepsilon_0}. \end{aligned} \tag{1.21}$$

By using the definition of $\kappa_{z1} = \sqrt{k_x^2 - k_0^2\mu_1\varepsilon_1}, \kappa_{z2} = \sqrt{k_x^2 - k_0^2\mu_2\varepsilon_2}$, from Eqs. (1.14) and (1.15) we can get the dispersion relation for TM mode as follows:

$$k_x = k_0\sqrt{\frac{\varepsilon_1\varepsilon_2}{\varepsilon_1 + \varepsilon_2}}. \tag{1.22}$$

By assuming that the permittivity of medium 2, ε_2, is a constant, and the permittivity of medium 1, ε_1, is the Drude dielectric function, we can get the dispersion relation of the TM mode or SP on the flat surface as follows:

$$k_x = k_0\sqrt{\frac{\varepsilon_2(\omega^2 - \omega_p^2)}{\omega^2 - \omega_p^2 + \varepsilon_2}}. \tag{1.23}$$

In Fig. 1.6, we show a plot of frequency ω of TM mode as a function of wavevector k_x on the boundary of silver and air ($\omega_{\mathrm{sp,air}}$) and on the boundary of silver and silica ($\omega_{\mathrm{sp,silica}}$). The ω of TM mode is linear to wave vector for the small frequency corresponding to mid or lower infra-red. For larger wave vector, the ω approaches constant value of

$$\omega_{\mathrm{sp}} = \frac{\omega_{\mathrm{p}}}{\sqrt{1 + \varepsilon_2}}, \tag{1.24}$$

where ω_{p} is the bulk plasmon frequency given in Eq. (1.9). It is noted that, for the boundary with vacuum, the $\omega = \omega_{\mathrm{sp}}/\sqrt{2}$. As is shown in Fig. 1.6, the dispersion of TM mode is located at the right side of dispersion of light, which means that we have an EM wave that is confined to the surface of the metal [12].

Chapter 2

Electromagnetic wave on cylindrical system

In this chapter we will derive the expression of EM field in the cylindrical coordinate for calculating the dispersion relation of SP and the enhancement of the electric field, which is given in the Chapter 3. Simple cases of SP in a solid cylinder without a hollow core was first examined to help identifying two types of SPs on metallic cylinder. Then the solution of SPs on a metallic cylinder with a hollow core is presented.

2.1 The Helmholtz equation in cylindrical system

In this section we solve the SP modes on a solid metallic cylinder. In a cylindrical coordinate, we consider a metallic cylinder with radius a that is infinitely long in the z-direction, with the z axis as the axis of the cylinder, as is shown in Fig. 2.1.

We start from the Maxwell equations for electric and magnetic field ($\mathbf{E}$ and $\mathbf{H}$) without any charge or current:

$$\boldsymbol{\nabla} \cdot \mathbf{E} = 0, \tag{2.1}$$

$$\boldsymbol{\nabla} \cdot \mathbf{H} = 0, \tag{2.2}$$

$$\boldsymbol{\nabla} \times \mathbf{E} = -\mu_0 \mu_r \frac{\partial \mathbf{H}}{\partial t}, \tag{2.3}$$

$$\boldsymbol{\nabla} \times \mathbf{H} = \varepsilon_0 \varepsilon_r \frac{\partial \mathbf{E}}{\partial (t)}. \tag{2.4}$$

Fig. 2.1: Fig/samplesolid.PNG

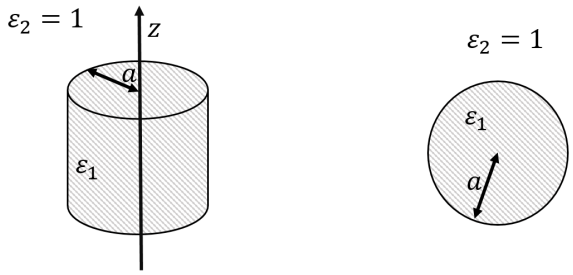

Figure 2.1 A metallic cylinder with relative permittivity ε_1 and radius a in a vacuum background.

For simplicity, for the rest part of this thesis we only consider case when the materials are nonmagnetic, $\mu_r \approx 1$. By taking curl to Eqs. (2.3) and (2.4), we get the following equations:

$$\boldsymbol{\nabla} \times \boldsymbol{\nabla} \times \mathbf{E} = -\mu_0 \frac{\partial}{\partial t} \boldsymbol{\nabla} \times \mathbf{H}, \tag{2.5}$$

$$\boldsymbol{\nabla} \times \boldsymbol{\nabla} \times \mathbf{H} = \varepsilon_0 \varepsilon_r \frac{\partial}{\partial t} \boldsymbol{\nabla} \times \mathbf{E} \tag{2.6}$$

Using the formula from vector calculus as follows:

$$\boldsymbol{\nabla} \times \boldsymbol{\nabla} \times \mathbf{E} = \boldsymbol{\nabla}(\boldsymbol{\nabla} \cdot \mathbf{E}) - \nabla^2 \mathbf{E} = -\nabla^2 \mathbf{E}, \tag{2.7}$$

$$\boldsymbol{\nabla} \times \boldsymbol{\nabla} \times \mathbf{H} = \boldsymbol{\nabla}(\boldsymbol{\nabla} \cdot \mathbf{H}) - \nabla^2 \mathbf{H} = -\nabla^2 \mathbf{H}, \tag{2.8}$$

and substituting Eqs. (2.7) and (2.3) to Eq. (2.5), Eqs. (2.8) and (2.4) to Eq.(2.6), we get the wave equation of the EM field, which is known as the Helmholtz equations:

$$\nabla^2 \mathbf{E} - \mu_0 \varepsilon_0 \varepsilon_r \frac{\partial^2 \mathbf{E}}{\partial t^2} = 0, \tag{2.9}$$

$$\nabla^2 \mathbf{H} - \mu_0 \varepsilon_0 \varepsilon_r \frac{\partial^2 \mathbf{H}}{\partial t^2} = 0. \tag{2.10}$$

Let us write Eqs. (2.9) and (2.10) in cylindrical coordinate by using the Laplace operator ∇^2 in cylindrical coordinate as follows:

$$\nabla^2 f = \frac{1}{\rho} \frac{\partial}{\partial \rho} (\rho \frac{\partial \boldsymbol{f}}{\partial \rho}) + \frac{1}{\rho^2} \frac{\partial^2 \boldsymbol{f}}{\partial \phi^2} + \frac{\partial^2 \boldsymbol{f}}{\partial z^2}, \tag{2.11}$$

thus, we get the Helmholtz equations in cylindrical coordinate as follows:

$$\frac{1}{\rho}\frac{\partial}{\partial\rho}(\rho\frac{\partial \boldsymbol{E}}{\partial\rho})+\frac{1}{\rho^2}\frac{\partial^2 \boldsymbol{E}}{\partial\phi^2}+\frac{\partial^2 \boldsymbol{E}}{\partial z^2}-\mu_0\varepsilon_0\varepsilon_r\frac{\partial^2 \boldsymbol{E}}{\partial t^2}=0, \tag{2.12}$$

$$\frac{1}{\rho}\frac{\partial}{\partial\rho}(\rho\frac{\partial \boldsymbol{H}}{\partial\rho})+\frac{1}{\rho^2}\frac{\partial^2 \boldsymbol{H}}{\partial\phi^2}+\frac{\partial^2 \boldsymbol{H}}{\partial z^2}-\mu_0\varepsilon_0\varepsilon_r\frac{\partial^2 \boldsymbol{H}}{\partial t^2}=0, \tag{2.13}$$

Let us assume a solution for Eq. (2.12) written as follows:

$$\mathbf{E}(\rho,\varphi,z,t)=\mathbf{E}_\rho(\rho)\Phi(\varphi)Z(z)e^{-i\omega t}, \tag{2.14}$$

$$=[E_\rho(\rho)\hat{\boldsymbol{\rho}}+\mathbf{E}_\varphi(\rho)\hat{\boldsymbol{\varphi}}+E_z(\rho)\hat{\mathbf{z}}]\Phi(\varphi)Z(z)e^{-i\omega t}. \tag{2.15}$$

For simplicity, here we write $\mathbf{E}_\rho(\rho)$ as $\mathbf{E}_\rho$, $E_\rho(\rho)$ as E_ρ, $E_\phi(\rho)$ as E_ϕ, $E_z(\rho)$ as E_z, $\Phi(\varphi)$ as Φ, $Z(z)$ as Z. By substituting Eqs. (2.15) into Eqs. (2.12), we get the following equation

$$\mathbf{E}_\rho\Phi Ze^{-i\omega t}\left[\frac{1}{\mathbf{E}_\rho\rho}\frac{\partial}{\partial\rho}\left(\rho\frac{\partial\mathbf{E}_\rho}{\partial\rho}\right)+\frac{1}{\Phi\rho^2}\frac{\partial^2\Phi}{\partial\varphi^2}+\frac{1}{Z}\frac{\partial^2 Z}{\partial z^2}-\mu_0\varepsilon_0\varepsilon_r\omega^2\right]=0. \tag{2.16}$$

To get a nontrivial solution, we have $\mathbf{E}(\rho,\varphi,z,t)=\mathbf{E}_\rho(\rho)\Phi(\varphi)Z(z)e^{-i\omega t}\neq 0$, and by also noticing that the speed of light in materials is given by $v_r=v_0\sqrt{\frac{1}{\varepsilon_r}}=\sqrt{\frac{1}{\varepsilon_0\varepsilon_r\mu_0}}$, from Eq. (2.16) we can get,

$$\begin{aligned}\frac{1}{\mathbf{E}_\rho\rho}\frac{\partial}{\partial\rho}\left(\rho\frac{\partial\mathbf{E}}{\partial\rho}\right)+\frac{1}{\Phi\rho^2}\frac{\partial^2\Phi}{\partial\varphi^2}+\frac{1}{Z}\frac{\partial^2 Z}{\partial z^2}&=-\mu_0\varepsilon_0\varepsilon_r\omega^2\leftrightarrow\\ \frac{1}{\mathbf{E}_\rho}\left(\frac{1}{\rho}\frac{\partial\mathbf{E}}{\partial\rho}+\frac{\partial^2\mathbf{E}_\rho}{\partial\rho^2}\right)+\frac{1}{\Phi\rho^2}\frac{\partial^2\Phi}{\partial\varphi^2}&=-\frac{1}{Z}\frac{\partial^2 Z}{\partial z^2}-\frac{\omega^2}{v_r^2},\end{aligned} \tag{2.17}$$

Eqs. (2.17) contains independent variables z, ϕ and ρ, we then separate Eq. (2.17) into three equations to solve it. Let us define the radial wave vector k_ρ as follows:

$$k_\rho^2=\frac{1}{Z}\frac{\partial^2 Z}{\partial z^2}+\frac{\omega^2}{v_r^2}. \tag{2.18}$$

By substituting Eq. (2.18) into Eq. (2.17), we can get the following equations.

$$\begin{aligned}\frac{1}{\mathbf{E}_\rho}\left(\frac{1}{\rho}\frac{\partial\mathbf{E}_\rho}{\partial\rho}+\frac{\partial^2\mathbf{E}_\rho}{\partial\rho^2}\right)+\frac{1}{\Phi\rho^2}\frac{\partial^2\Phi}{\partial\varphi^2}&=-k_\rho^2\leftrightarrow\\ \frac{1}{\mathbf{E}_\rho}\left(\rho\frac{\partial\mathbf{E}_\rho}{\partial\rho}+\rho^2\frac{\partial^2\mathbf{E}_\rho}{\partial\rho^2}\right)+k_\rho^2\rho^2&=-\frac{1}{\Phi}\frac{\partial^2\Phi}{\partial\varphi^2},\end{aligned} \tag{2.19}$$

By defining the azimuthal wave number n as follows:

$$n^2=-\frac{1}{\Phi}\frac{\partial^2\Phi}{\partial\varphi^2}, \tag{2.20}$$

then by substituting Eq. (2.20) into Eq. (2.19), we can get the following equations:

$$\frac{1}{\mathbf{E}_\rho}\left(\rho\frac{\partial \mathbf{E}_\rho}{\partial \rho}+\rho^2\frac{\partial^2 \mathbf{E}_\rho}{\partial \rho^2}\right)+k_\rho^2\rho^2=n^2 \leftrightarrow$$
$$\rho\frac{\partial \mathbf{E}_\rho}{\partial \rho}+\rho^2\frac{\partial^2 \mathbf{E}_\rho}{\partial \rho^2}+\left(k_\rho^2\rho^2-n^2\right)\mathbf{E}_\rho=0. \tag{2.21}$$

Eqs. (2.18), (2.20) and (2.21) is a group of second order differential equations describing any propagating electric wave in cylindrical coordinate. By defining the wave vector on z direction: $k_z=\sqrt{\omega^2/v_r^2-k_\rho^2}$, the equation group can be written as follows:

$$\frac{\partial^2 \Phi}{\partial \varphi^2}+n^2\Phi=0, \tag{2.22}$$
$$\frac{\partial^2 Z}{\partial z^2}+k_z^2 Z=0, \tag{2.23}$$
$$\rho^2\frac{\partial^2 \mathbf{E}_\rho}{\partial \rho^2}+\rho\frac{\partial \mathbf{E}_\rho}{\partial \rho}+\left(k_\rho^2\rho^2-n^2\right)\mathbf{E}_\rho=0. \tag{2.24}$$

From Eq. (2.22) we can get one of the nontrivial solutions for Φ as follows:

$$\Phi=A_n e^{in\varphi}, \tag{2.25}$$

where A_n is a constant that is determined by boundary conditions. It is noted that Φ has periodic boundary condition as follows:

$$\Phi(\varphi_1)=\Phi(\varphi_1+2\pi). \tag{2.26}$$

From the Eq. (2.26) we understand the range of value for angular wave number n given as follows:

$$n\in\mathbb{Z}, \tag{2.27}$$

where $\mathbb{Z}$ denotes the integer set.

From Eq. (2.23) we can get a nontrival solution for Z as follows:

$$Z=B_1e^{ik_z z}+B_2e^{-ik_z z}. \tag{2.28}$$

By defining $x=\sqrt{k_\rho}\rho$ in Eq. (2.24), we get the following equation for $\mathbf{E}_\rho$

$$x^2\frac{\partial^2 \mathbf{E}_\rho}{\partial x^2}+x\frac{\partial \mathbf{E}_\rho}{\partial x}+\left(x^2-n^2\right)\mathbf{E}_\rho=0, \tag{2.29}$$

which is a Bessel differential equations.

By substituting the Eqs. (2.25) and (2.28) into Eqs. (2.14), we arrive at the expression of a electromagnetic wave in cylindrical coordinate as follows:

$$\mathbf{E} = \mathbf{E}_\rho A_n e^{in\varphi}(B_1 e^{ik_z z} + B_2 e^{-ik_z z})e^{-i\omega t}. \tag{2.30}$$

It is worth noticing that Eq. (2.13) has a same structure as the Eq. (2.12), from which we conclude that a nontrivial solution of $\mathbf{H}$ has a similar structure given as follows:

$$\mathbf{H} = \mathbf{H}_\rho A'_n e^{in\varphi}(B'_1 e^{ik_z z} + B'_2 e^{-ik_z z})e^{-i\omega t}. \tag{2.31}$$

Equation (2.29) is a Bessel equation, which means that the nontrivial solution for $\mathbf{E}_\rho$ should be a linear combination of the Bessel functions, as is the solution for $\mathbf{H}_\rho$. The specific expressions of $\mathbf{E}_\rho$ and $\mathbf{H}_\rho$ is discussed in the following sections.

2.1.1 Surface plasmons propagating in azimuthal direction

We first consider a surface plasmon that propagates in the azimuthal direction, as is depicted in Fig. 2.2 (a). We start by considering the a EM wave that does not propagate in the z-direction, i.e. $k_z = 0$. The expressions for EM waves become:

$$\mathbf{E} = \mathbf{E}_\rho A_n e^{in\varphi} e^{-i\omega t}, \tag{2.32}$$

$$\mathbf{H} = \mathbf{H}_\rho A'_n e^{in\varphi} e^{-i\omega t}, \tag{2.33}$$

where

$$\mathbf{E}_\rho = E_\rho \hat{\rho} + E_\varphi \hat{\varphi} + E_z \hat{\mathbf{z}}, \tag{2.34}$$

$$\mathbf{H}_\rho = H_\rho \hat{\rho} + H_\varphi \hat{\varphi} + H_z \hat{\mathbf{z}}. \tag{2.35}$$

By substituting the expressions from Eqs. (2.32) and (2.33) into the Faraday law: Eq. (2.3), we can get the numerical relationship between the different components of EM fields. By noting that $\frac{\partial}{\partial z} = 0$, $\frac{\partial}{\partial \varphi} = in$, $\frac{\partial}{\partial t} = -i\omega$, the relation between H_ρ and E_z can then be derived as follows:

$$\begin{aligned} \frac{1}{\rho}\frac{\partial}{\partial \varphi}\hat{\rho} - \frac{\partial}{\partial z}\hat{\rho} &= -\mu_0 \frac{\partial}{\partial t} H_\rho e^{in\varphi} e^{-i\omega t}\hat{\rho}, \\ \Rightarrow \frac{n}{\rho} &= \mu_0 \omega H_\rho. \end{aligned} \tag{2.36}$$

The expression of H_φ and H_z can be derived as follows:

$$-\frac{\partial E_z}{\partial \rho} = i\mu_0\omega H_\varphi, \tag{2.37}$$

$$\frac{1}{\rho}E_\varphi + \frac{\partial E_\varphi}{\partial \rho} - \frac{in}{\rho}E_\rho = i\mu_0\omega H_z. \tag{2.38}$$

By substituting the expressions from Eqs. (2.32) and (2.33) into the Ampere law: Eqs. (2.4), we arrive at the following equations

$$\frac{n}{\rho}H_z = -\varepsilon_0\varepsilon_r\omega E_\rho, \tag{2.39}$$

$$-\frac{\partial H_z}{\partial \rho} = -i\varepsilon_0\varepsilon_r\omega E_\varphi, \tag{2.40}$$

$$\frac{1}{\rho}H_\varphi + \frac{\partial H_\varphi}{\partial \rho} - \frac{in}{\rho}H_\rho = -i\varepsilon_0\varepsilon_r\omega E_z. \tag{2.41}$$

Equations (2.36) - (2.41) can be separated into two equation groups that are linearly independent to each other, each group describes an independent wave mode. One of the equation groups is given as follows:

$$\begin{aligned} \frac{n}{\rho}H_z &= -\varepsilon_0\varepsilon_r\omega E_\rho, \\ -\frac{\partial H_z}{\partial \rho} &= -i\varepsilon_0\varepsilon_r\omega E_\varphi, \\ \frac{1}{\rho}E_\varphi + \frac{\partial E_\varphi}{\partial \rho} - \frac{in}{\rho}E_\rho &= i\mu_0\omega H_z. \end{aligned} \tag{2.42}$$

Equation group (2.42) describes an electromagnetic wave mode that has a component of electric field only in z-direction, as is depicted in Fig. 2.2 (a). Regarding the fact that this EM wave mode propagates along the circumference of the cylinder i.e. along the φ direction and this mode has a magnetic field only in perpendicular to that of the propagation direction, hence this EM wave mode is an azimuthal transverse magnetic (TM) wave mode. As is explained in Chapter 1, the TM mode describes a surface plasmon mode if the wave is confined to the surface.

The other equation group is given as follows:

$$\begin{aligned} \frac{n}{\rho} &= \mu_0\omega H_\rho, \\ -\frac{\partial E_z}{\partial \rho} &= i\mu_0\omega H_\varphi, \\ \frac{1}{\rho}E_\varphi + \frac{\partial E_\varphi}{\partial \rho} - \frac{in}{\rho}E_\rho &= i\mu_0\omega H_z. \end{aligned} \tag{2.43}$$

Fig. 2.2: Fig/solidSP.PNG

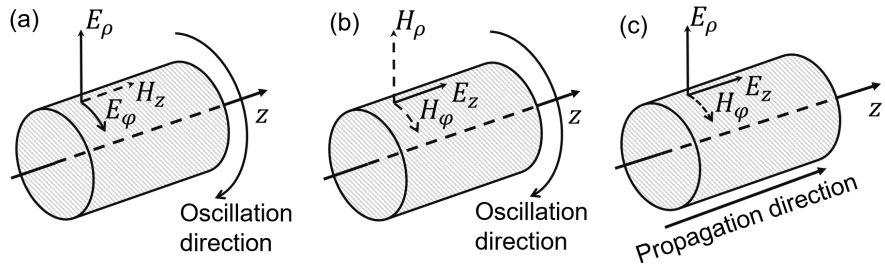

Figure 2.2 (a) A TM mode that oscillates in azimuthal direction, (b) A TE mode that oscillates in azimuthal direction, (c) A TM mode that propagates in axial direction

Equation group (2.43) describes a wave mode with a component of magnetic field only in direction perpendicular to propagation direction, as is shown in Fig. 2.2 (b), hence this equation group describes an TE mode that oscillates around the cylinder axis. This TE mode will not be discussed further in this thesis.

We will now try to derive the expressions of EM wave of a surface TM mode. We already know that both $\mathbf{E}_\rho$ and $\mathbf{H}_\rho$ should be a solution of the Bessel differential equation [Eq. (2.29)], and the solutions also need to satisfy the equation group (2.42) to be a TM mode. By assuming that the H_z component has the following expression:

$$H_z = b'_n J_n(k_\rho \rho) + b_n Y_n(k_\rho \rho), \tag{2.44}$$

where b'_n and b_n are constants, J_n and Y_n are n-th orders Bessel functions of first and second respectively. It is worth mentioning that since $n \in \mathbb{Z}$, all the Bessel functions we are going to discuss in this thesis are the Bessel functions of integer orders. For the Eq. (2.44) to be a surface mode, it must satisfy the boundary condition as follows:

$$H_z = 0 \qquad \text{at } \rho \to \infty, \tag{2.45}$$

$$H_z \neq \pm\infty \qquad \text{at } \rho = 0. \tag{2.46}$$

For the EM field at the outside of the metallic cylinder, i.e $\rho > a$, the EM wave propagates in vacuum, where the permittivity $\varepsilon_2 = \varepsilon_0$, the argument for the Bessel functions in Eq. (2.44) which is written as follows:

$$x = k_{\rho(2)}\rho = \sqrt{\omega^2 \varepsilon_0 \mu_0}\rho, \tag{2.47}$$

is a positive real number or 0. Noticing that with a real argument, only the second kind of the Bessel function could meet the boundary condition Eq. (2.45) [32], hence

$b'_n = 0$, expression of the magnetic field outside the cylinder is then:

$$H_z^{(2)} = b_n Y_n(k_{\rho(2)}\rho). \tag{2.48}$$

For the expressions of EM field inside the cylinder, which have its relative permittivity ε_{r1} described by Eq. (1.8). For simplicity let us first assume that there is no damping: $\gamma = 0$. With the parameters we were using: $\varepsilon_b = 5.97$, $\omega_d/(2\pi) = 2113.6$ THz. Noticing that with $\omega < 5.4 \times 10^{15}$ Hz, or $\lambda > 350$ nm, which covers common optical frequency, ε_1 is always a negative number. With a negative ε_{r1}, arguments of the Bessel functions described in Eq. (2.47) is always an imaginary value. Noticing that for any arbitrary real value x, the Bessel functions J_n and Y_n are represented by the modified Bessel functions $I_n(x)$ and $K_n(x)$ as follows [33]:

$$J_n(ix) = e^{ni\frac{\pi}{2}} I_n(x), \tag{2.49}$$

$$Y_n(ix) = e^{(n+1)i\frac{\pi}{2}} I_n(x) - \frac{\pi}{2} e^{ni\frac{\pi}{2}} K_n(x). \tag{2.50}$$

By defining the extinction coefficient z_ρ as follows:

$$z_\rho^2 = k_z^2 - \omega^2 \varepsilon_0 \varepsilon_r \mu_0, \tag{2.51}$$

$$z_\rho = ik_\rho, \tag{2.52}$$

expression of H_z as given in Eq. (2.44) can also be represented as linear combination of the modified Bessel functions:

$$\begin{aligned} H_z &= b'_n J_n(iz_{\rho(1)}\rho) + b_n Y_n(iz_{\rho(1)}\rho) \\ &= a_n I_n(z_{\rho(1)}\rho) + a'_n K_n(z_{\rho(1)}\rho). \end{aligned} \tag{2.53}$$

Because the K_n is infinite at $\rho = 0$, to satisfy the boundary condition at $\rho = 0$, a'_n in Eq. 2.53 is 0. The magnetic component inside the metallic cylinder is then written as follows:

$$H_z^{(1)} = a_n I_n(z_{\rho(1)}\rho). \tag{2.54}$$

By substituting Eqs. (2.48) and (2.54) into Eqs. (2.39) and (2.40), we will get the

components for the TM wave mode of the n-th order as follows:

$$H_z^{(1)} = a_n I_n(z_{\rho(1)}\rho), \tag{2.55}$$

$$E_\varphi^{(1)} = -ia_n \frac{1}{\varepsilon_0 \varepsilon_1 \omega} \frac{\partial I_n(z_{\rho(1)}\rho)}{\partial \rho}, \tag{2.56}$$

$$E_\rho^{(1)} = -a_n \frac{n}{\rho \varepsilon_0 \varepsilon_1 \omega} I_n(z_{\rho(1)}\rho), \tag{2.57}$$

for $\rho < a$.

$$H_z^{(2)} = b_n Y_n(k_{\rho(2)}\rho), \tag{2.58}$$

$$E_\varphi^{(2)} = -ib_n \frac{1}{\varepsilon_0 \varepsilon_2 \omega} \frac{\partial Y_n(k_{\rho(2)}\rho)}{\partial \rho}, \tag{2.59}$$

$$E_\rho^{(2)} = -b_n \frac{n}{\rho \varepsilon_0 \varepsilon_2 \omega} Y_n(k_{\rho(2)}\rho), \tag{2.60}$$

for $\rho > a$.

Now we need to consider the boundary conditions to get the dispersion relation of the azimuthal TM mode. From the boundary conditions at the surface of the cylinder i.e. at $\rho = a$ given as follows:

$$H_z^{(1)} = H_z^{(2)}, \tag{2.61}$$

$$E_\varphi^{(1)} = E_\varphi^{(2)}, \tag{2.62}$$

we can get the dispersion relation for the azimuthal TM mode by substituting Eqs. (2.55) - (2.60) to Eqs. (2.61) and (2.62) as follows:

$$\varepsilon_2 \frac{\partial I_n(z_{\rho(1)}\rho)}{\partial \rho} Y_n(k_{\rho(2)}\rho) - \frac{\partial Y_n(k_{\rho(2)}\rho)}{\partial \rho} I_n(z_{\rho(1)}\rho) = 0. \tag{2.63}$$

2.1.2 Surface plasmons propagating along axial direction

On a cylinder, an SP is refereed as an axial SP if it propagates only along the axis of the cylinder with wave vector k_z and doesn't propagates in azimuthal direction, i.e. $n = 0$, as is depicted in 2.2 (b). For simplicity, we will start by considering an EM wave that propagates in positive z-direction. Expressions of EM field described in Eqs. (2.30) and (2.31) then become:

$$\mathbf{E} = \mathbf{E}_\rho (B_1 e^{ik_z z}) e^{-i\omega t}, \tag{2.64}$$

$$\mathbf{H} = \mathbf{H}_\rho (B_1' e^{ik_z z}) e^{-i\omega t} \tag{2.65}$$

where $\mathbf{E}_\rho$ and $\mathbf{H}_\rho$ are given in Eqs. (2.34) and (2.35).

Noticing that $\frac{\partial}{\partial\varphi} = 0$, $\frac{\partial}{\partial z} = ik_z$, $\frac{\partial}{\partial\omega} = 0$, by substituting the Eq. (2.64) into the Faraday law: Eq. (2.3), we get the following equations:

$$-k_z E_\varphi = \mu_0 \omega H_\rho, \tag{2.66}$$

$$ik_z E_\rho - \frac{\partial E_z}{\partial \rho} = i\mu_0 \omega H_\varphi, \tag{2.67}$$

$$\frac{1}{\rho} E_\varphi + \frac{\partial E_\varphi}{\partial \rho} = i\mu_0 \omega H_z. \tag{2.68}$$

By substituting Eq. (2.64) into the Ampere law: Eq. (2.4), we can get the following equations:

$$k_z H_\varphi = \varepsilon \omega E_\rho, \tag{2.69}$$

$$ik_z H_\rho - \frac{\partial H_z}{\partial \rho} = i\varepsilon_0 \varepsilon_r \omega E_\varphi, \tag{2.70}$$

$$\frac{1}{\rho} H_\varphi + \frac{\partial H_\varphi}{\partial \rho} = i\varepsilon_0 \varepsilon_r \omega E_z. \tag{2.71}$$

Noticing that with the EM wave propagating in the z-axis, Eqs. (2.67), (2.69) and (2.71) now forms a group of equations with common variables H_φ, E_ρ and E_z, which describes a TM mode, as is describes in Fig. 2.2 (c). The radial wave vector: Eq. (2.18) outside the cylinder is written as follows:

$$k_{\rho(2)}^2 = \omega^2 \epsilon_0^2 \mu_0^2 - k_z^2, \tag{2.72}$$

to get a surface confined wave, $k_{\rho(2)}$ need to be imaginary, i.e. $k_z > k_0$. As is discuss in section 2.1, E_z for outside of cylinder, which is a solution of the Bessel differential equation [Eq. (2.21)], can be written as the linear combination of the modified Bessel functions I_n and K_n with arguments $z_{\rho(2)}\rho = -ik_\rho(2)\rho$. As it should satisfy the boundary condition at $\rho \to \infty$, the solution of the E_z should therefore be

$$E_z^{(1)} = c_1 I_0(z_{\rho(1)}\rho), \quad \rho < a, \tag{2.73}$$

$$E_z^{(2)} = c_2 K_0(z_{\rho(2)}\rho). \quad \rho \geqslant a. \tag{2.74}$$

Here, c_1 and c_2 are constant. By substituting Eqs. (2.73) and (2.74) into Eqs. (2.67),

(2.69) and (2.71), we can get the components of EM fields for axial SP as follows:

$$E_z^{(1)} = c_1 I_0(z_{\rho(1)}\rho), \tag{2.75}$$

$$H_\varphi^{(1)} = -ic_1 \frac{\varepsilon_0\varepsilon_1\omega}{k_{\rho(1)}^2} \frac{\partial I_0(z_{\rho(1)}\rho)}{\partial\rho}. \tag{2.76}$$

$$E_\rho^{(1)} = -ic_1 \frac{k_z}{k_{\rho(1)}^2} \frac{\partial I_0(z_{\rho(1)}\rho)}{\partial\rho}, \tag{2.77}$$

for $\rho < a$, and

$$E_z^{(2)} = c_2 K_0(z_{\rho(1)}\rho), \tag{2.78}$$

$$H_\varphi^{(2)} = -ic_2 \frac{\varepsilon_0\omega}{k_{\rho(2)}^2} \frac{\partial K_0(z_{\rho(2)}\rho)}{\partial\rho}, \tag{2.79}$$

$$E_\rho^{(2)} = -ic_2 \frac{k_z}{k_{\rho(2)}^2} \frac{\partial K_0(z_{\rho(2)}\rho)}{\partial\rho}, \tag{2.80}$$

for $\rho \geqslant a$.

From the boundary conditions at the surface of the cylinder i.e. at $\rho = a$ given as follows:

$$E_z^{(1)} = E_z^{(2)}, \tag{2.81}$$

$$H_\varphi^{(1)} = H_\varphi^{(2)}, \tag{2.82}$$

we can hence get the dispersion relation of the axial SP by substituting Eqs. (2.75) - (2.80) to Eqs. (2.81) and (2.82) as follows:

$$\varepsilon_1 k_{\rho(2)}^2 \frac{\partial I_0(z_{\rho(1)}\rho)}{\partial\rho} K_0(z_{\rho(2)}\rho) - k_{\rho(1)}^2 \frac{\partial K_0(z_{\rho(2)}\rho)}{\partial\rho} I_0(z_{\rho(1)}\rho) = 0, \tag{2.83}$$

2.1.3 Elliptical surface plasmon

We have finished the discussion of the SP that is either purely axial (characterized by $n = 0$) or purely azimuthal (characterized by $k_z = 0$), but in most of the experiments both types of modes are excited. Wave modes with both $k_z \neq 0$ and $n \neq 0$ are refereed as an elliptical mode in this thesis, as mathematically such mode propagates in both axial and azimuthal directions. In this section we are going to discuss the mathematical behavior of such mode.

A wave propagating in the cylindrical coordinate is described by Eqs. (2.30) and (2.31) and for simplicity, let us consider that the wave only propagates in the positive

z-direction, i.e. $B_2 = 0$ and $B_2' = 0$. By substituting the Eqs. (2.30) and (2.31) into the Ampere law: Eq. (2.4), we can get the following equations [34]:

$$\frac{n}{\rho}H_z - k_z H_\varphi = -\varepsilon_0\varepsilon_r\omega E_\rho, \tag{2.84}$$

$$ik_z H_\rho - \frac{\partial H_z}{\partial \rho} = -i\varepsilon_0\varepsilon_r\omega E_\varphi, \tag{2.85}$$

$$\frac{1}{\rho}H_\varphi + \frac{\partial H_\varphi}{\partial \rho} - \frac{in}{\rho}H_\rho = -i\varepsilon_0\varepsilon_r\omega E_z. \tag{2.86}$$

By substituting Eqs. (2.30) and (2.31) into the Faraday law: Eq. (2.3), we get the following equations:

$$\frac{n}{\rho}E_z - k_z E_\varphi = \mu_0\omega H_\rho, \tag{2.87}$$

$$ik_z E_\rho - \frac{\partial E_z}{\partial \rho} = i\mu_0\omega H_\varphi, \tag{2.88}$$

$$\frac{1}{\rho}E_\varphi + \frac{\partial E_\varphi}{\partial \rho} - \frac{in}{\rho}E_\rho = \mu_0\omega H_z. \tag{2.89}$$

Equations (2.84) - (2.89) cannot be separated into TE or TM mode, and must be solved together. The solutions of Eqs. (2.84) - (2.89) are written as follows [35, 36]:

$$\mathbf{E}_\rho = \sum_{n=-\infty}^{\infty}\mathbf{E}_{n\rho} = \sum_{n=-\infty}^{\infty}\frac{(-i)^n}{k_{\rho(0)}}E_0\left[a_n\mathbf{M}_n + b_n\mathbf{N}_n\right]e^{in\varphi}e^{ik_z z}, \tag{2.90}$$

$$\mathbf{H}_\rho = \sum_{n=-\infty}^{\infty}\mathbf{H}_{n\rho} = -\sqrt{\frac{\varepsilon_r\varepsilon_0}{\mu_0}}\sum_{n=-\infty}^{\infty}\frac{(-i)^n}{k_{\rho(0)}}E_0\left[a_n\mathbf{N}_n + b_n\mathbf{M}_n\right]e^{in\varphi}e^{ik_z z}, \tag{2.91}$$

where E_0, a_n and b_n are the constant to be obtained by the boundary conditions, $k_{\rho(0)}$ is the k_ρ of the vacuum, and the $\mathbf{N}_n$ and $\mathbf{M}_n$ are given as follows:

$$\mathbf{M}_n = \boldsymbol{\nabla}\times\hat{\boldsymbol{z}}B_n(x) = \frac{in}{\rho}B_n(x)\hat{\boldsymbol{\rho}} - k_\rho\frac{\partial B_n(x)}{\partial x}\hat{\boldsymbol{\varphi}}. \tag{2.92}$$

$$\begin{aligned}\mathbf{N}_n &= \frac{\boldsymbol{\nabla}\times\mathbf{M}_n}{\varepsilon_0\varepsilon_r\mu_0\omega^2}\\ &= -\frac{ik_z k_\rho}{\sqrt{\varepsilon_0\varepsilon_r\mu_0}\omega}\frac{\partial B_n(x)}{\partial x}\hat{\boldsymbol{\rho}} + \frac{k_z n}{\rho\sqrt{\varepsilon_0\varepsilon_r\mu_0}\omega}B_n(x)\hat{\boldsymbol{\varphi}} + \frac{k_\rho^2}{\sqrt{\varepsilon_0\varepsilon_r\mu_0}\omega}B_n(x)\hat{\boldsymbol{z}},\end{aligned} \tag{2.93}$$

where the B_n is the Bessel function whose explicit expression is determined by its argument x and boundary condition at $\rho = 0$ and $\rho \to \infty$. When x is expressed with $x = z_\rho\rho$, $k_{\rho(0)}$ is the k_ρ in vacuum, B_n is written as follows:

$$B_n = \alpha_n I_n(z_{\rho(2)}\rho) \quad \rho < a, \tag{2.94}$$

$$B_n = \beta_n K_n(z_{\rho(2)}\rho) \quad \rho \geqslant a. \tag{2.95}$$

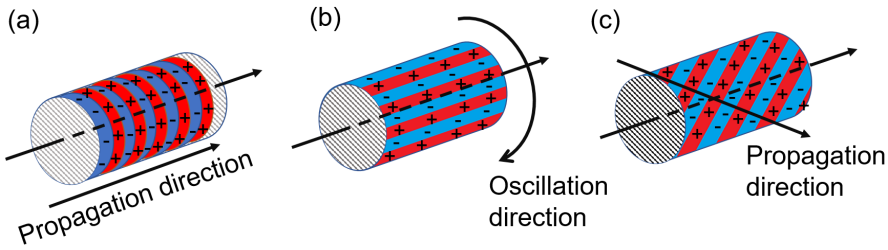

Figure 2.3 (a) SP that propagates only in axial direction. (b) SP that oscillates in azimuthal direction. (c) SP that propagates in spiral direction, or an elliptical SP.

If x is expressed by $x = k_\rho \rho = iz_\rho$, noticing from Eq. (2.49), I_n can be represented with J_n, and K_n can be represented by the first kind of the Hankel function $h_n^{(1)}$ as follows [37]:

$$K_n(x) = \frac{\pi i}{2} e^{n\pi i/2} h_n^{(1)}(ix). \tag{2.96}$$

Therefore, Eqs. (2.94) and 2.95 can also be written as the Bessel and the Hankel functions as follows:

$$B_n = \alpha'_n J_n(k_{\rho(2)}\rho) \qquad \rho < a, \tag{2.97}$$

$$B_n = \beta'_n h_n^{(1)}(k_{\rho(2)}\rho) \qquad \rho \geqslant a. \tag{2.98}$$

We will now discuss the relation between the elliptical solution and the pure azimuthal/axial modes decribed in previous sections. When $k_z = 0$, i.e. the wave is propagating only in azimuthal direction, Eqs. (2.92) and (2.93) change into the following expressions :

$$\mathbf{M}_n = \frac{in}{\rho} B_n(x)\hat{\boldsymbol{\rho}} - k_\rho \frac{\partial B_n(x)}{\partial x}\hat{\boldsymbol{\varphi}}. \tag{2.99}$$

$$\mathbf{N}_n = \frac{k_\rho^2}{\sqrt{\varepsilon_0 \varepsilon_r \mu_o}\omega} B_n(x)\hat{\boldsymbol{z}}. \tag{2.100}$$

By substituting Eqs. (2.99) and (2.100) into Eqs. (2.90) and (2.91), and for simplicity,

Fig. 2.3: Fig/solid-ellip.PNG

we denote $E_n = \frac{(-i)^n}{k_{\rho(0)}} E_0$, we get the following expressions:

$$\mathbf{E}_{n\rho} = a_n E_n \left[\frac{in}{\rho} B_n(x)\hat{\boldsymbol{\rho}} - k_\rho \frac{\partial B_n(x)}{\partial x}\hat{\boldsymbol{\varphi}} \right] e^{in\varphi} + b_n E_n \left[\frac{k_\rho^2}{\sqrt{\varepsilon_0 \varepsilon_r \mu_o}\omega} B_n(x)\hat{\boldsymbol{z}} \right] e^{in\varphi}, \tag{2.101}$$

$$\mathbf{H}_{n\rho} = -a_n E_n \sqrt{\frac{\varepsilon_r \varepsilon_0}{\mu_0}} \left[\frac{k_\rho^2}{\sqrt{\varepsilon_0 \varepsilon_r \mu_0}\omega} B_n(x)\hat{\boldsymbol{z}} \right] e^{in\varphi} - b_n E_n \sqrt{\frac{\varepsilon_r \varepsilon_0}{\mu_0}} \left[\frac{in}{\rho} B_n(x)\hat{\boldsymbol{\rho}} - k_\rho \frac{\partial B_n(x)}{\partial x}\hat{\boldsymbol{\varphi}} \right] e^{in\varphi}. \tag{2.102}$$

It is not hard to notice that Eqs. (2.101) and (2.102) represent the linear combination of the azimuthal TM and TE mode, as when $b_n = 0$, Eqs. (2.101) and (2.102) describes an azimuthal TM mode, and when $a_n = 0$, Eqs. (2.101) and (2.102) describes an azimuthal TE mode.

When $n = 0$ and $k_z \neq 0$, i.e. the wave is propagating only in axial direction. Eqs. (2.92) and (2.93) change into the following equation:

$$\mathbf{M}_n = -k_\rho \frac{\partial B_0(x)}{\partial \rho}\hat{\boldsymbol{\varphi}}. \tag{2.103}$$

$$\mathbf{N}_n = -\frac{ik_z k_\rho}{\sqrt{\varepsilon_0 \varepsilon_r \mu_o}\omega} \frac{\partial B_0(x)}{\partial x}\hat{\boldsymbol{\rho}} + \frac{k_\rho^2}{\sqrt{\varepsilon_0 \varepsilon_r \mu_o}\omega} B_0(x)\hat{\boldsymbol{z}}, \tag{2.104}$$

By substituting Eqs (2.103) and (2.104) into the Eqs. (2.90) and (2.91), we will get the following expressions:

$$\mathbf{E}_{0\rho} = a_0 E_0 \left[k_\rho \frac{\partial B_0(x)}{\partial x}\hat{\boldsymbol{\varphi}} \right] e^{ik_z z} + b_0 E_0 \left[-\frac{ik_z k_\rho}{\sqrt{\varepsilon_0 \varepsilon_r \mu_o}\omega} \frac{\partial B_0(x)}{\partial x}\hat{\boldsymbol{\rho}} + \frac{k_\rho^2}{\sqrt{\varepsilon_0 \varepsilon_r \mu_o}\omega} B_0(x)\hat{\boldsymbol{z}} \right] e^{ik_z z}, \tag{2.105}$$

$$\mathbf{H}_{0\rho} = a_0 E_0 \sqrt{\frac{\varepsilon_r \varepsilon_0}{\mu_0}} \left[-\frac{ik_z k_\rho}{\sqrt{\varepsilon_0 \varepsilon_r \mu_o}\omega} \frac{\partial B_0(x)}{\partial x}\hat{\boldsymbol{\rho}} + \frac{k_\rho^2}{\sqrt{\varepsilon_0 \varepsilon_r \mu_o}\omega} B_0(x)\hat{\boldsymbol{z}} \right] e^{ik_z z} - b_0 E_0 \sqrt{\frac{\varepsilon_r \varepsilon_0}{\mu_0}} \left[-k_\rho \frac{\partial B_0(x)}{\partial x}\hat{\boldsymbol{\varphi}} \right] e^{ik_z z}, \tag{2.106}$$

It is apparent that Eqs. (2.105) and (2.106) describe an axial TE mode when $b_0 = 0$ or an axial TM mode when $a_0 = 0$. The relation between axial TM mode, azimuthal TM mode and elliptical TM mode is described in Fig. (2.3).

From the above calculation, it is reasonable to say that an axial wave mode is an elliptical wave mode with $n = 0$, $k_z \neq 0$ and an azimuthal wave mode is a elliptical

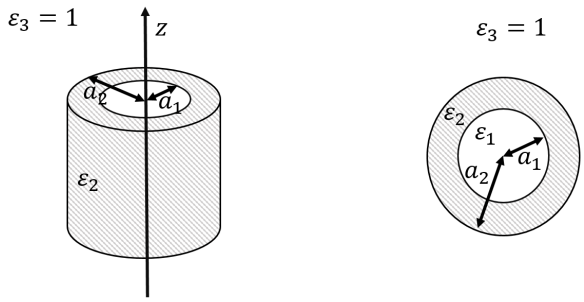

Figure 2.4 A infinite long metallic hollow cylinder with a dielectric core, with inner radius a_1 and outer radius a_2, in a vacuum background.

wave mode with $k_z = 0$. The description of the axial and azimuthal surface modes are both obtained within the description of the elliptical wave mode: Eqs. (2.90) - (2.98).

2.2 Surface modes on hollow cylinder

In this section, we discuss the SP (TM mode) in a hollow cylinder, which is our main topic. Let us consider a hollow cylinder that is infinitely long in axial direction, with inner radius a_1 and outer radius a_2, as is shown in Fig. 2.4. The relative permittivities of the dielectric core and of the vacuum background are given by $\varepsilon_1 \geqslant 1$ and $\varepsilon_3 = 1$, respectively, while the relative permittivity of the metallic tube ε_2 is given by the Eq. (1.8). As is discussed in previous sections, the EM waves in cylindrical coordinate and both types of SPs are described with Eqs. (2.90) - (2.93). By assuming the argument of the Bessel equations: $x = k_\rho \rho$, from the boundary condition Eqs. (2.45) and (2.46), the B_n in Eqs. (2.92) is expressed as follows:

$$B_n^{(1)} = J_n(k_{\rho^{(1)}}\rho) \qquad \rho < a_1, \tag{2.107}$$

$$B_n^{(2)} = \alpha_n J_n(k_{\rho^{(2)}}\rho) + \gamma_n Y_n(k_{\rho(2)}\rho) \qquad a_1 < \rho \leqslant a_2, \tag{2.108}$$

$$B_n^{(3)} = h_n^{(1)}(k_{\rho^{(3)}}\rho) \qquad a_2 \leqslant \rho, \tag{2.109}$$

where α_n and γ_n are parameters to be solved.

Now we calculate the dispersion relation of the elliptical modes from the boundary conditions in the hollow cylinder, from which we can also get the dispersion relation

Fig. 2.4: Fig/hollowsample.PNG

for the axial and azimuthal TM modes. For simplicity we denote the relative wave vector $k_r = \sqrt{\varepsilon_0 \varepsilon_r \mu_0}\omega$. By substituting Eqs. (2.107)-(2.109) into Eqs. (2.92) and (2.93), $\mathbf{M}_n$ and $\mathbf{N}_n$ for $\rho < a_1$ and $\rho \geqslant a_2$ are then written as the follows:

$$\begin{aligned}
&\mathbf{M}_n^{(i)} = \frac{in}{\rho} B_n(k_\rho^{(i)}\rho)\hat{\boldsymbol{\rho}} - k_\rho^{(i)} \frac{\partial B_n(k_\rho^{(i)}\rho)}{\partial(k_\rho^{(i)}\rho)}\hat{\boldsymbol{\varphi}} \\
\Leftrightarrow\quad &\mathbf{M}_n^{(i)} \equiv M_{n\rho}^{(i)}\hat{\boldsymbol{\rho}} + M_{n\varphi}^{(i)}\hat{\boldsymbol{\varphi}} \qquad (2.110) \\
&\mathbf{N}_n^{(i)} = -\frac{ik_z k_\rho^{(i)}}{k_r^{(i)}} \frac{\partial B_n(k_\rho^{(i)}\rho)}{\partial(k_\rho^{(i)}\rho)}\hat{\boldsymbol{\rho}} + \frac{k_z n}{\rho k_r^{(i)}} B_n(k_\rho^{(i)}\rho)\hat{\boldsymbol{\varphi}} + \frac{k_\rho^{(i)2}}{k_r^{(i)}} B_n(k_\rho^{(i)}\rho)\hat{\boldsymbol{z}} \\
\Leftrightarrow\quad &\mathbf{N}_n^{(i)} \equiv N_{n\rho}^{(i)}\hat{\boldsymbol{\rho}} + N_{n\varphi}^{(i)}\hat{\boldsymbol{\varphi}} + N_{nz}^{(i)}\hat{\boldsymbol{z}}, \qquad (2.111)
\end{aligned}$$

where $i = 1$ or 3 for $\rho < a_1$ or $\rho \geqslant a_2$, while $\mathbf{M}_n$ and $\mathbf{N}_n$ for $a_1 \leqslant \rho < a_2$ are written as follows:

$$\begin{aligned}
&\mathbf{M}_n^{(2)} = \left[\alpha_n \frac{in}{\rho} J_n(k_\rho^{(2)}\rho) + \gamma_n \frac{in}{\rho} Y_n(k_\rho^{(2)}\rho)\right]\hat{\boldsymbol{\rho}} \\
&\qquad + \left[-\alpha_n k_\rho^{(2)} \frac{\partial J_n(k_\rho^{(2)}\rho)}{\partial(k_\rho^{(2)}\rho)} - \gamma_n k_\rho^{(2)} \frac{\partial Y_n(k_\rho^{(2)}\rho)}{\partial(k_\rho^{(2)}\rho)}\right]\hat{\boldsymbol{\varphi}} \\
\Leftrightarrow\quad &\mathbf{M}_n^{(2)} \equiv \left[\alpha_n M_{n\rho J}^{(2)} + \gamma_n M_{n\rho Y}^{(2)}\right]\hat{\boldsymbol{\rho}} + \left[\alpha_n M_{n\varphi Y}^{(2)} + \gamma_n M_{n\varphi J}^{(2)}\right]\hat{\boldsymbol{\varphi}}, \qquad (2.112) \\
&\mathbf{N}_n^{(1)} = \left[-\alpha_n \frac{ik_z k_\rho^{(2)}}{k_r^{(2)}} \frac{\partial J_n(k_\rho^{(2)}\rho)}{\partial(k_\rho^{(2)}\rho)} - \gamma_n \frac{ik_z k_\rho^{(2)}}{k_r^{(2)}} \frac{\partial Y_n(k_\rho^{(2)}\rho)}{\partial(k_\rho^{(2)}\rho)}\right]\hat{\boldsymbol{\rho}} \\
&\qquad + \left[\alpha_n \frac{k_z n}{\rho k_r^{(2)}} J_n(k_\rho^{(2)}\rho) + \gamma_n \frac{k_z n}{\rho k_r^{(2)}} Y_n(k_\rho^{(2)}\rho)\right]\hat{\boldsymbol{\varphi}} \\
&\qquad + \left[\alpha_n \frac{k_\rho^{(2)2}}{k_r^{(2)}} J_n(k_\rho^{(2)}\rho) + \gamma_n \frac{k_\rho^{(2)2}}{k_r^{(2)}} Y_n(k_\rho^{(2)}\rho)\right]\hat{\boldsymbol{z}} \\
\Leftrightarrow\quad &\mathbf{N}_n^{(1)} \equiv \left[\alpha_n N_{n\rho J}^{(2)} + \gamma_n N_{n\rho Y}^{(2)}\right]\hat{\boldsymbol{\rho}} + \left[\alpha_n N_{n\varphi Y}^{(2)} + \gamma_n N_{n\varphi J}^{(2)}\right]\hat{\boldsymbol{\varphi}} + \left[\alpha_n N_{nzY}^{(2)} + \gamma_n N_{nzJ}^{(2)}\right]\hat{\boldsymbol{z}}. \\
&\qquad (2.113)
\end{aligned}$$

For simplicity, we denote the propagation phase as $P = e^{in\varphi}e^{ik_z z}$ and $\beta_r = \sqrt{\frac{\varepsilon_r \varepsilon_1}{\mu_0}}$. By substituting Eqs. (2.110)-(2.113) into Eqs. (2.90) and (2.91), expressions for EM

field in the three regions are given as follows:

$$E_{n\rho}^{(i)} = E_n \left[a_n^{(i)} M_{n\rho}^{(i)} + b_n^{(i)} N_{n\rho}^{(i)} \right] P,$$
$$E_{n\varphi}^{(i)} = E_n \left[a_n^{(i)} M_{n\varphi}^{(i)} + b_n^{(i)} N_{n\varphi}^{(i)} \right] P, \qquad E_{nz}^{(i)} = E_n \left[b_n^{(i)} N_{nz}^{(i)} \right] P, \tag{2.114}$$
$$H_{n\rho}^{(i)} = \beta_r^{(i)} E_n \left[a_n^{(i)} N_{n\rho}^{(i)} + b_n^{(i)} M_{n\rho}^{(i)} \right] P,$$
$$H_{n\varphi}^{(i)} = \beta_r^{(i)} E_n \left[a_n^{(i)} N_{n\varphi}^{(i)} + b_n^{(i)} M_{n\varphi}^{(i)} \right] P, \quad H_{nz}^{(i)} = \beta_r^{(i)} E_n \left[a_n^{(i)} N_{nz}^{(i)} \right] P, \tag{2.115}$$

where $i = 1$ or 3 for $\rho < a_1$ or $\rho \geqslant a_2$, and

$$E_{n\rho}^{(2)} = E_n \left[a_n^{(2)} \alpha_n M_{n\rho J}^{(2)} + a_n^{(2)} \gamma_n M_{n\rho Y}^{(2)} + b_n^{(2)} \alpha_n N_{n\rho J}^{(2)} + b_n^{(2)} \gamma_n N_{n\rho Y}^{(2)} \right] P,$$
$$E_{n\varphi}^{(2)} = E_n \left[a_n^{(2)} \alpha_n M_{n\varphi Y}^{(2)} + a_n^{(2)} \gamma_n M_{n\varphi J}^{(2)} + b_n^{(2)} \alpha_n N_{n\varphi Y}^{(2)} + b_n^{(2)} \gamma_n N_{n\varphi J}^{(2)} \right] P,$$
$$E_{nz}^{(2)} = E_n \left[b_n^{(2)} \alpha_n N_{nzY}^{(2)} + b_n^{(2)} \gamma_n N_{nzJ}^{(2)} \right] P, \tag{2.116}$$
$$H_{n\rho}^{(2)} = \beta_r^{(2)} E_n \left[a_n^{(2)} \alpha_n N_{n\rho J}^{(2)} + a_n^{(i)} \gamma_n N_{n\rho Y}^{(2)} + b_n^{(2)} \alpha_n M_{n\rho J}^{(2)} + b_n^{(2)} \gamma_n M_{n\rho Y}^{(2)} \right] P,$$
$$H_{n\varphi}^{(2)} = \beta_r^{(2)} E_n \left[a_n^{(2)} \alpha_n N_{n\varphi Y}^{(2)} + a_n^{(2)} \gamma_n N_{n\varphi J}^{(2)} + b_n^{(2)} \alpha_n M_{n\varphi Y}^{(2)} + b_n^{(2)} \gamma_n M_{n\varphi J}^{(2)} \right] P,$$
$$H_{nz}^{(2)} = \beta_r^{(2)} E_n \left[a_n^{(2)} \alpha_n N_{nzY}^{(2)} + a_n^{(2)} \gamma_n N_{nzJ}^{(2)} \right] P, \tag{2.117}$$

for $a_2 > \rho \geqslant a_1$.

The boundary conditions on a hollow cylinder are written as follows:

$$\left.\begin{array}{ll} E_\varphi^{(1)} = E_\varphi^{(2)} & E_z^{(1)} = E_z^{(2)} \\ H_\varphi^{(1)} = H_\varphi^{(2)}, & H_z^{(1)} = H_z^{(2)} \end{array}\right\} \quad \text{at } \rho = a_1, \tag{2.118}$$

$$\left.\begin{array}{ll} E_\varphi^{(2)} = E_\varphi^{(3)} & E_z^{(2)} = E_z^{(3)} \\ H_\varphi^{(2)} = H_\varphi^{(3)}, & H_z^{(2)} = H_z^{(3)} \end{array}\right\} \quad \text{at } \rho = a_2. \tag{2.119}$$

By substituting Eqs. (2.114)-(2.117) into Eqs. (2.118) and (2.119), we get the secular equation for solving the dispersion relations of wave modes.

First let us discuss the dispersion relation for an axial TM mode in a hollow cylinder. As is discussed in the previous sections, the EM fields for axial TM mode should have $n = 0$ and $a_n^{(i)} = 0$. By substituting $n = 0$ and $a_n^{(i)} = 0$ into Eqs. (2.110)-(2.113),

we will get the following matrix equation:

$$\begin{bmatrix} N_{0z}^{(1)}(a_1) & -N_{0zJ}^{(2)}(a_1) & -N_{0zY}^{(2)}(a_1) & 0 \\ \beta_r^{(1)} M_{0\varphi}^{(1)}(a_1) & -\beta_r^{(2)} M_{0\varphi J}^{(2)}(a_1) & -\beta_r^{(2)} M_{0\varphi Y}^{(2)}(a_1) & 0 \\ 0 & N_{0zJ}^{(2)}(a_2) & N_{0zY}^{(2)}(a_2) & -N_{0z}^{(3)}(a_2) \\ 0 & \beta_r^{(2)} M_{0\varphi J}^{(2)}(a_2) & \beta_r^{(2)} M_{0\varphi Y}^{(2)}(a_2) & -\beta_r^{(3)} M_{0\varphi}^{(3)}(a_2) \end{bmatrix} \begin{bmatrix} b_0^{(1)} \\ b_0^{(2)} \alpha_0 \\ b_0^{(2)} \gamma_0 \\ b_0^{(3)} \end{bmatrix} = 0. \tag{2.120}$$

Equation (2.120) is a matrix equation for SP mode in hollow cylinder. By solving the secular equation of Eq. (2.120), we get the dispersion relation of the axial SP mode on the hollow cylinder.

In Fig. (2.5) we show the dispersion relation of axial SP in hollow cylinder with certain geometries. Because there exists two surfaces, then there could be 2 types of SP mode, since the charge oscillation on inner and outer surfaces can have the same or opposite polarity. In Fig. (2.5), the solid line corresponds to SP mode with the opposite polarity, while the dashed line corresponds to the SP mode with the same polarity [9].

To excite the axial SP modes in a hollow metallic cylinder, the incident light and the SP mode must have the same frequency ω and the same parallel wave vector components k_z. For incident light coming from the vacuum background, this can be achieved only when incident light is parallel to that of the axis of the cylinder, as when $k_z = k$. But as light is a transverse wave, when the light is parallel to the axis, there would be no E_z component of the incident light to excite the axial SP. Hence the axial SP cannot be excited with an incident light comes directly from vacuum [32, 29]. To excite the axial SP mode with light, a so-called Otto or Kretschmann geometry is needed [12].

Now we discuss the case for an azimuthal SP mode. From the discussion in previous section, we know that azimuthal SP mode should have $k_z = 0$, $b_n^{(i)} = 0$. By substituting $k_z = 0$ and $b_n^{(i)} = 0$ into Eqs. (2.110)-(2.113), we will get matrix equation for azimuthal

Fig. 2.5: Fig/disper-axi.png

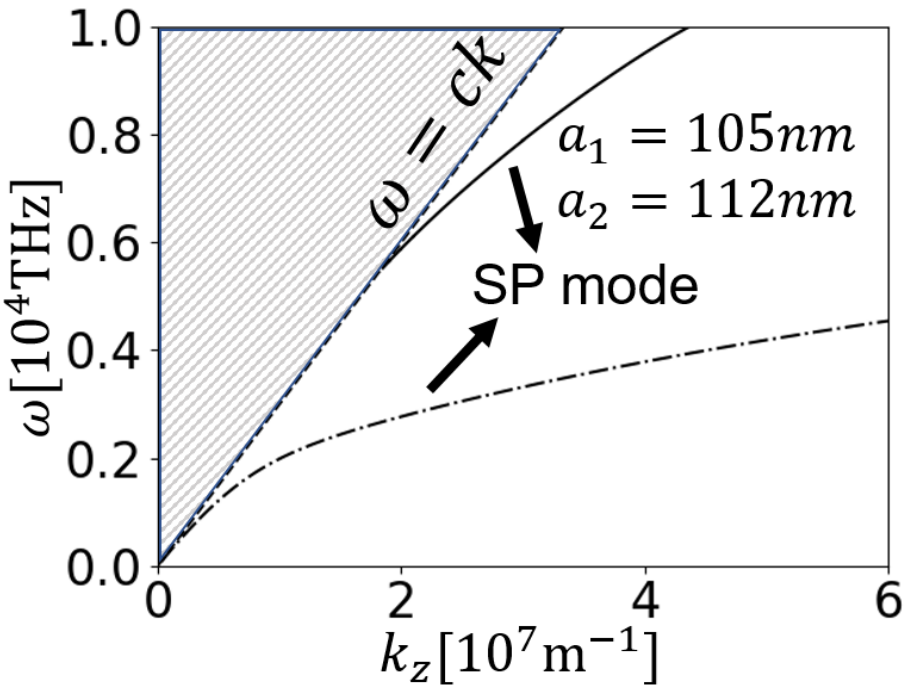

Figure 2.5 Dispersion relation of the axial surface plasmon on the metallic cylinder with geometry parameters of $a_1 = 105$ nm, $a_2 = 112$ nm. Shadowed region is the value range of k_z of possible incident lights in vacuum. The strait dashed line is the dispersion relations of the light that is propagating on the z direction.

SP modes as follows:

$$\begin{bmatrix} M_{n\varphi}^{(1)}(a_1) & -M_{n\varphi J}^{(2)}(a_1) & -M_{n\varphi Y}^{(2)}(a_1) & 0 \\ \beta_r^{(1)} N_{nz}^{(1)}(a_1) & -\beta_r^{(2)} N_{nzJ}^{(2)}(a_1) & -\beta_r^{(2)} N_{nzY}^{(2)}(a_1) & 0 \\ 0 & M_{n\varphi J}^{(2)}(a_2) & M_{n\varphi Y}^{(2)}(a_2) & -M_{n\varphi}^{(3)}(a_2) \\ 0 & \beta_r^{(2)} N_{nzJ}^{(2)}(a_2) & \beta_r^{(2)} N_{nzY}^{(2)}(a_2) & -\beta_r^{(3)} M_{nz}^{(3)}(a_2) \end{bmatrix} \begin{bmatrix} a_n^{(1)} \\ a_n^{(2)} \alpha_n \\ a_n^{(2)} \gamma_n \\ a_n^{(3)} \end{bmatrix} = 0. \tag{2.121}$$

Eq. (2.121) is a matrix equation that determines the azimuthal SP mode. By solving the matrix equations of Eq. (2.121), we can get the dispersion relation for the azimuthal SP mode. In Fig. (2.6), we show the dispersion relation of the azimuthal SP mode with $n = 1$. The frequency ω is plotted as a functions of $d = a_2 - a_1$ with several given inner radius a_1. As d increases, ω approaches a constant value.

Fig. 2.6: Fig/disper-azi.png

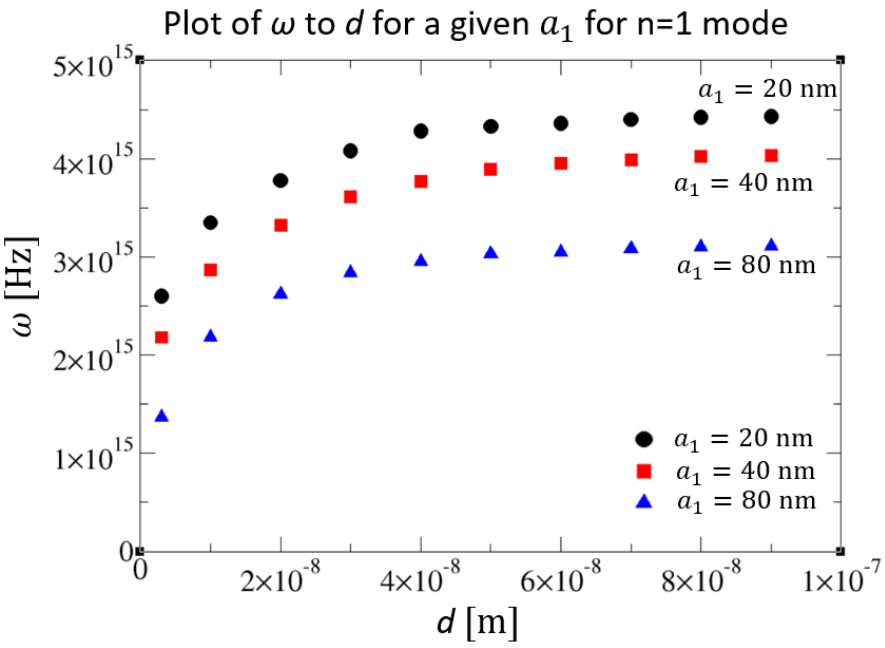

Figure 2.6 Dispersion relation of n=1 order azimuthal surface plasmon mode with several given a_1, given as function $d = a_2 - a_1$.

2.3 Enhancement and the incident light

In this section we discuss the expression of the incident light that excites the surface plasmon and generates the near field enhancement. For a pure azimuthal mode to be excited, incident light should obey that $k_z = 0$, which mean a light with propagation direction perpendicular to that of the axis of the cylinder. Further more, to excite an azimuthal SP mode, the incident light must contains the same EM field components with that of the SP mode: E_ρ, E_φ and H_z, which can only be achieved by a planar polarized light that is perpendicularly polarized to that of the axis of the cylinder, as is shown in Fig. 2.7 (b). For simplicity let us assume that the light propagates in x direction and polarized in y direction, the electric field intensity of the light is E_0. The expressions of such EM wave are written as follows [38]:

$$\mathbf{E}^{(inc)} = e^{-(ikx+\omega t)} E_0 \hat{\boldsymbol{y}} = E_0 e^{-ik\rho\cos\varphi - i\omega t}(\sin\varphi\hat{\boldsymbol{\rho}} + \cos\varphi\hat{\boldsymbol{\varphi}}), \tag{2.122}$$

$$\mathbf{H}^{(inc)} = \beta_0 E_0 e^{-ik\rho\cos\varphi - i\omega t}\hat{\boldsymbol{z}}. \tag{2.123}$$

By noting that the plane wave can be expanded into the Bessel functions as follows:

$$e^{-ik\rho\cos\varphi} = \sum_{n=-\infty}^{\infty} (-i)^n J_n(k\rho) e^{in\varphi}, \tag{2.124}$$

Eqs. (2.122) and (2.123) are expanded in terms of of the Bessel functions:

$$E_{n\rho}^{(inc)} = E_0(-i)^n J_n(k\rho)\sin\varphi P = E_n k_{\rho(0)} E_{n\rho}^{(inc)\prime} P, \tag{2.125}$$

$$E_{n\varphi}^{(inc)} = E_0(-i)^n J_n(k\rho)\cos\varphi P = E_n k_{\rho(0)} E_{n\varphi}^{(inc)\prime} P, \tag{2.126}$$

$$H_{nz}^{(inc)} = \beta_r^{(3)} E_0(-i)^n J_n(k\rho) P = E_n k_{\rho(0)} H_{nz}^{(inc)\prime} P. \tag{2.127}$$

By adding of the incident light on the outside of the cylinder, the boundary conditions for azimuthal SP mode would change into the following forms:

$$\begin{array}{cc} E_\varphi^{(1)} = E_\varphi^{(2)}, & H_z^{(1)} = H_z^{(2)}, \quad \text{at } \rho = a_1, \\ E_\varphi^{(2)} = E_\varphi^{(3)} + E_\varphi^{(inc)}, & H_z^{(1)} = H_z^{(2)} + E_\varphi^{(inc)}, \quad \text{at } \rho = a_2. \end{array} \tag{2.128}$$

By substituting the Eqs. (2.116)-(2.117) and Eqs. (2.125)-(2.127) with arguments $k_z = 0$, $b_n = 0$ into Eqs. (2.128) , for simplicity, we denote that $c_n = a_{(2)\alpha_n}$ and $d_n = a_{(2)\gamma_n}$, we can get a matrix equation as follows:

$$\begin{bmatrix} M_{n\varphi}^{(1)}(a_1) & -M_{n\varphi J}^{(2)}(a_1) & -M_{n\varphi Y}^{(2)}(a_1) & 0 \\ \beta_r^{(1)} N_{nz}^{(1)}(a_1) & -\beta_r^{(2)} N_{nzJ}^{(2)}(a_1) & -\beta_r^{(2)} N_{nzY}^{(2)}(a_1) & 0 \\ 0 & M_{n\varphi J}^{(2)}(a_2) & M_{n\varphi Y}^{(2)}(a_2) & -M_{n\varphi}^{(3)}(a_2) \\ 0 & \beta_r^{(2)} N_{nzJ}^{(2)}(a_2) & \beta_r^{(2)} N_{nzY}^{(2)}(a_2) & -\beta_r^{(3)} M_{nz}^{(3)}(a_2) \end{bmatrix} \begin{bmatrix} a_n^{(1)} \\ c_n \\ d_n \\ a_n^{(3)} \end{bmatrix}$$

$$= \begin{bmatrix} 0 \\ 0 \\ E_{n\varphi}^{(inc)\prime}(a_2) \\ H_{nz}^{(inc)\prime}(a_2) \end{bmatrix}. \tag{2.129}$$

For any given a_1, a_2 and ω, we can solve the Eqs. (2.129) to get the parameters $a_n^{(1)}$, c_n, d_n and $a_n^{(3)}$. By substituting the parameters into the solution of the Eqs. (2.116)-(2.117), we can get the expressions of the EM field components of azimuthal SP modes in i-th regions of n-th order:$E_{n\varphi}^{(i)}$, $E_{n\rho}^{(i)}$ and $H_{nz}^{(i)}$, with electric field is then written as:

$$\mathbf{E} = \sum_{n=-\infty}^{\infty} \left[E_n \rho^{(i)} \hat{\rho} + E_n \varphi^{(i)} \hat{\varphi} \right] \tag{2.130}$$

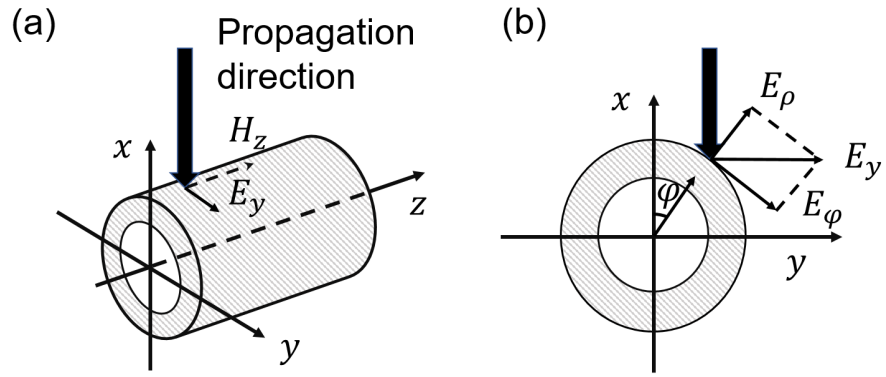

Figure 2.7 (a) An incident light that is perpendicular to the axis, with wave vector E_x and H_z. (b) E_x can be decomposed as E_ρ and E_φ.

for $\rho < a_2$, and

$$\mathbf{E} = \sum_{n=-\infty}^{\infty} \left[E_n \rho^{(i)} \hat{\rho} + E_n \varphi^{(i)} \hat{\varphi} + E_{n\rho}^{(inc)} \hat{\rho} + E_{n\varphi}^{(inc)} \hat{\varphi} \right] \tag{2.131}$$

for $a_2 \leqslant \rho$.

Now we have the expression for the electric field under the incident light, we move on to discuss the enhancement of electric field in hollow cylinder.

Fig. 2.7: Fig/incident.png

Chapter 3

Enhancement of electric field around the hollow cylinder

In this chapter we show the enhancement of the electric field on the metallic hollow cylinder especially the spatial distribution of the electric field enhancement in the cylinder. By showing the spatial distribution of the enhancement, especially the enhancement inside the hollow cylinder, we can see that there exists a strong and homogeneous enhancement of electric field in the hollow of the cylinder.

3.1 The spatial distribution of electric field in the hollow cylinder

The enhancement is defined as $|\mathbf{E}/E_0|$, where $\mathbf{E}$ is the electric field given in Eq. (2.130) and (2.131), which expression includes the expression of the incident light. As is expressed in Sec. we focus on the pure azimuthal mode. In Fig. 3.1, we show the $|\mathbf{E}/E_0|$ as a function of position in xy plane with $a_1 = 20$ nm, $a_2 = 25$ nm and incident light frequency $\omega = 2870$ Thz. The top and left side figures show the $|\mathbf{E}/E_0|$ as a function of x at $y = 0$ and y with $x = 0$, respectively. As we can see, the electric field is enhanced more than 5 times close to the surface of the cylinder. It is noted that the polarization of incident electric field is in $x-$direction, that is why the maximum enhancement is at the boundary with $y = 0$. The enhancement inside the hollow cylinder is nearly uniform with enhancement more than 10 times. This

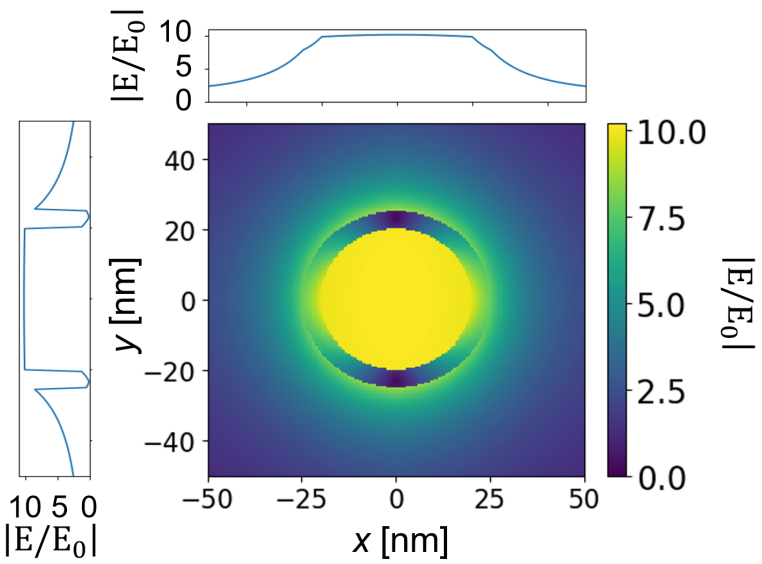

Figure 3.1 The enhancement of electric field as a function of position in xy plane. Here, we use $a_1 = 20$ nm, $a_2 = 25$ nm, $\omega = 2870$ Thz.

uniform enhancement is useful for applications such as by putting a sample inside the hollow cylinder for the Raman spectroscopy or heating of a sample. Thus, we will later focus on the enhancement inside the hollow cylinder, in particular at the center of the cylinder ($\rho = 0$).

In Fig. 3.2, we show the enhancement of electric field by several modes of electric field n. We find that the biggest enhancement comes from the $n = \pm 1$ mode by comparing Fig. 3.2 with Fig. 3.1, hence if the optimized enhancement is what we want, the excitation with the $n = \pm 1$ mode is the most important factor. A tendency we can find is that the enhancement decreases with increasing n as is shown in Fig. 3.2.

We now discuss the relation between light frequency and geometry parameters with the enhancement of electric field at the center of cylinder. A direct way to help understanding the relation is by plotting a two-dimensional plot of enhancement as a function of a_1 and a_2 as is shown in Fig. (3.3). In this plot, we try to find the largest enhancement for each pair of a_1 and a_2 by varying the frequency of incident light ω from 0 to 5.3×10^3 THz, and finding out the largest enhancement among them.

Fig. 3.1: Fig/figure3.png
Fig. 3.2: Fig/fig-compare.png

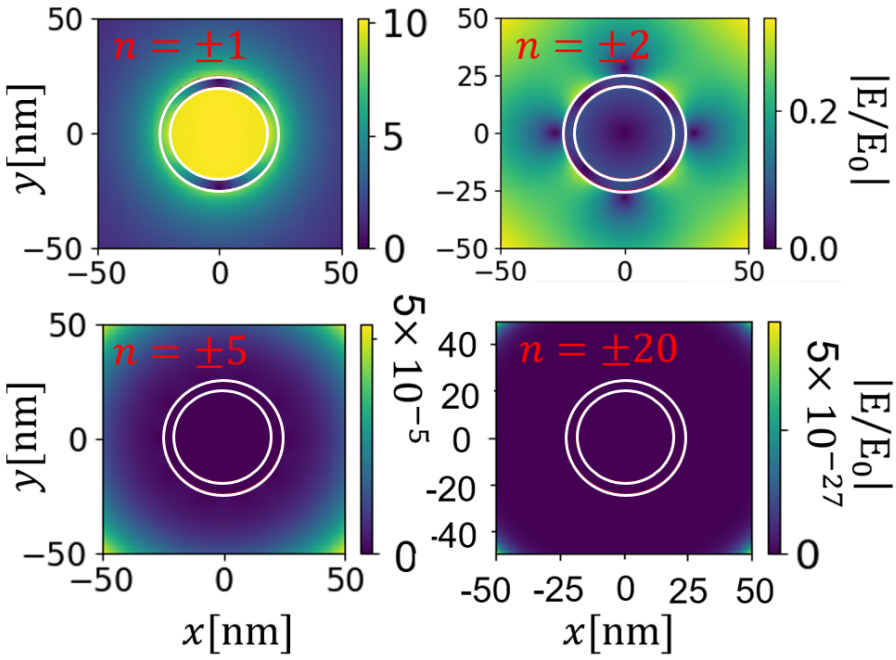

Figure 3.2 The contribution of different modes n to the total enhancement. Here, we use $a_1 = 20$ nm, $a_2 = 25$ nm, $\omega = 2870$ Thz. Notice how the enhancement decreases as n increases.

From Fig. (3.3), we could find that the largest enhancement, which is over 20, occurs in region a, where $a_1 \approx 5$ nm, and $a_2 \approx 30$ nm, and a generally high enhancement is expected when $a_1 < 10$ nm and $a_2 < 60$ nm. It is also observed that large enhancement occurs when wall is very thin ($d < 5$ nm), as is shown in region a. Result as shown Fig. (3.3) suggests that enhancement is higher with either very small inner radii: $a_1 < 10$ nm or with smaller thickness: $d < 5$ nm, But as we use the Drude model for calculating the dielectric function of the metal, and the Drude model is no more a good model for describing the behavior of the electrons when the size of the system less than 10 nm [39, 40], hence the large enhancement we get from calculation in region a and b with geometry size less than 10 nm could be inaccurate. We also need to consider technical difficulty in synthesizing cylinder which thickness less than 5 nm or with a inner radius less that 5 nm. We argue that simply suggesting that the best enhancement comes with the smallest diameters is not good enough, despite the result in Fig. (3.3) argues so.

Another area of comparable good enhancement is shown as region c in Fig. (3.3),

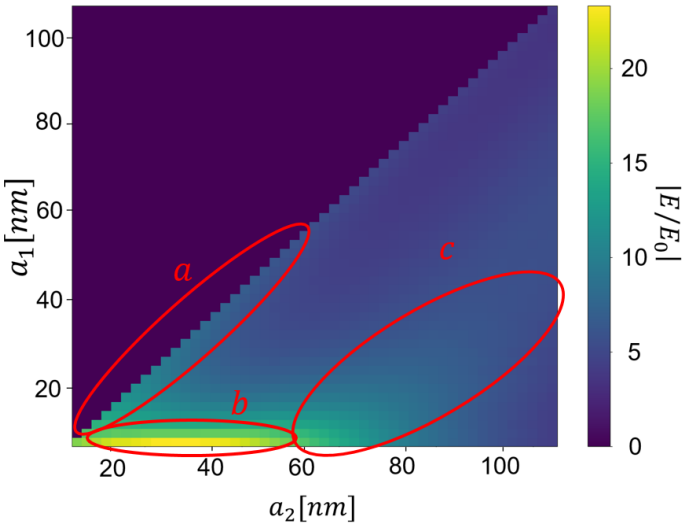

Figure 3.3 The largest possible enhancement of electric field as a function of a_1 and a_2. Region b

calculation results suggest that there is 5-10 times of enhancement in this area. It is however hard to find the optimized geometry for the largest enhancement from the result in Fig. (3.3). To find the largest enhancement and the optimized geometries, we need to find the mathematical relation between geometries, frequency and the enhancement. We will discuss the way to find such mathematical expression in the following chapter.

Fig. 3.3: Fig/2d-enhance.png

Chapter 4

The analytical expression of enhancement of electric field in a metallic hollow cylinder

In this chapter, we obtain analytical expression for enhancement as a function of geometry parameters and frequency. Such expression provides a mathematical relation between the enhancement, parameters, and incident light frequency, which would help to find optimized frequency for a given geometry, or vice versa. In all this chapter we will discuss the enhancement at the center of the cylinder, i.e. at $\rho = 0$.

4.1 The fitting of enhancement spectra

In Fig. 4.1, we show the total enhancement $|E/E_0|$ as a function of ω for several geometries. Here, we define thickness as $d = a_2 - a_1$. We can see that the geometry of hollow cylinder determines the enhancement spectrum, in particular, the frequency that gives maximum enhancement. Therefore, we can obtain a mathematical relation between then enhancement ratio, the geometry of hollow cylinder and the frequency of the light. From Fig. 4.1, we can find that despite the complex nature of the analytical expression of the electric field enhancement given by the solution of Eqs. (2.130) and (2.131), the relation between enhancement and frequency for a geometry may be fitted

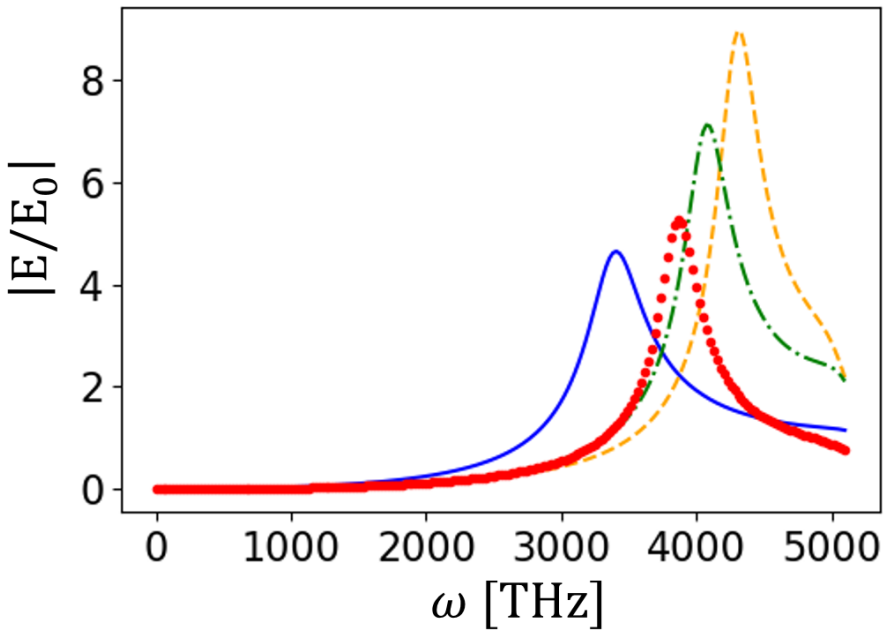

Figure 4.1 Total enhancement $|\mathbf{E}/E_0|$ of several geometries as a function of ω. Blue solid line: $a_1 = 40$ nm, $d = 20$ nm, orange dashed line: $a_1 = 15$ nm, $d = 30$ nm, green dot-dashed line: $a_1 = 20$ nm, $d = 25$ nm, red dot line: a_1=40 nm, $d = 40$ nm.

with a Lorentzian function $L(\omega)$ as follows:

$$L(\omega) = \frac{h}{1 + \left(\frac{\omega - \omega_0}{\gamma}\right)^2}. \tag{4.1}$$

We hence can represent the enhancement as a Lorentzian function with its argument ω, while the parameters of Lorentzian function can be taken as a function of geometry parameters a_1 and d, as is represents as follows:

$$\left|\frac{\mathbf{E}}{E_0}\right|(\omega, a_1, d) = \frac{h(a_1, d)}{1 + \left(\frac{\omega - \omega_0(a_1, d)}{\gamma(a_1, d)}\right)^2}, \tag{4.2}$$

where h corresponds to the maximum enhancement for a given geometry, ω_0 corresponds to the frequency that gives maximum enhancement i.e the resonance frequency., while γ gives the width of the spectrum. To find a general expression of enhancement, all the parameters in the Lorentzian function are also a function of a_1 and d. Thus, we conduct the fitting of the enhancement spectra with the Lorentzian function to

Fig. 4.1: Fig/1dcompare.png

obtain the parameters h, ω_0, γ for different geometries. Then, we can determine the mathematical relation between those parameters with the geometry. It is noted that we set a range of a_1 and d, 5 nm $< a_1 <$ 105 nm and 10 nm $< d <$ 110 nm, since we obtain good fitting with the Lorenztian within those range.

First we would try to find an expression for ω_0, which determines the frequency of the incident light when we have the maximum enhancement. We start by plotting the ω_0 as functions of d for some given a_1, as is shown in Fig. (4.2) as black dots for $a_1 = 20$ nm, red squares for $a_1 = 40$ nm, and blue triangles for $a_1 = 80$ nm. We find that for a given a_1, ω_0 could be roughly represented by the following function of d:

$$\omega_0(d, a_1) = p_1(a_1) + p_2(a_1)e^{-p_3(a_1)d} \tag{4.3}$$

The parameters of the function in Eq. (4.3), that is, p_1, p_2 and p_3, are functions of a_1. We repeat such procedure to the other two parameters h and γ. For a given a_1, relation between h and d could be fitted as a linear combination of an exponential function and a Lorentzian function as follows:

$$h(a_1, d) = \frac{p_4(a_1)}{1 + (\frac{d - p_5(a_1)}{p_6(a_1)})^2} + p_7(a_1)e^{-p_8(a_1)d} \tag{4.4}$$

For a given a_1, γ could be fitted as a following function:

$$\gamma(a_1, d) = p_9(a_1) + \frac{p_{10}(a_1)}{1 + (\frac{d - p_{11}(a_1)}{p_{12}(a_1)})^2}. \tag{4.5}$$

All parameters p_i in Eqs. (4.3), (4.4) and (4.5) can be expressed as function of a_1. We find that the expression of p_4 and p_7 can be expressed as exponential function as follows:

$$p_i(a_1) = \ m_1 + m_2 e^{m_3 a_1}. \tag{4.6}$$

where m_1, m_2 and m_3 are given as follows:

	m_1	m_2	m_3
p_4	5.46	8.55	-8×10^{-2}
p_7	0.94	14.45	-2.37×10^{-2}

While the expression of rest of the p_i is expressed as polynomial function given as follows:

$$p_i(a_1) = \ n_0 + n_1 a_1 + n_2 a_1^2 + n_3 a_1^3 + n_4 a_1^4 + n_5 a_1^5 + n_6 a_1^6, \tag{4.7}$$

where n_0-n_6 are given as follows:

	n_0	n_1	n_2	n_3	n_4	n_5	n_6
p_1	4.84×10^{1}	-2.22×10^{-2}	0	0	0	0	0
p_2	-1.57×10^{3}	-5×10^{1}	8.55×10^{-1}	-3.58×10^{-3}	0	0	0
p_3	2.47×10^{-1}	-2.02×10^{-2}	9.43×10^{-4}	-2.26×10^{-5}	2.93×10^{-7}	-1.95×10^{-9}	5.19×10^{-12}
p_5	3.62×10^{1}	1.75	-4.66×10^{-2}	4.75×10^{-4}	-1.72×10^{-6}	0	0
p_6	2.57×10^{1}	1.41	-3.94×10^{-2}	4.07×10^{-4}	-1.48×10^{-6}	0	0
p_8	5.46×10^{-3}	2.63×10^{-3}	-2.32×10^{-5}	0	0	0	0
p_9	6.44×10^{1}	1.54	-1.23×10^{-1}	2.81×10^{-3}	-2.83×10^{-5}	1.05×10^{-7}	0
p_{10}	3.06×10^{1}	1.1×10^{-1}	1.8×10^{-2}	-5.98×10^{-4}	7.16×10^{-6}	-2.89×10^{-8}	0
p_{11}	2.05×10^{1}	0.934	-3.24×10^{-2}	3.6×10^{-4}	-1.36×10^{-6}	0	0

In Eqs. (4.2)-(4.7), a_1 and d is given in unit of nm, and ω is given in unit of THz.

By substituting the expression of from Eqs. (4.6) and (4.7) into Eq. (4.3), we can get an approximate expression of ω_0 as a function of d and a_1. The calculated spectrum from Eqs. (4.3) is shown in Fig. (4.2) as lines, with data from the original fitting being plotted in Fig. (4.2) as dots, which shows a good fitting with the data of ω_0. It is worth noticing that ω_0 which represents the frequency for the highest enhancement as plotted in Fig. 4.2, which shows high correspondence with the frequency of azimuthal SP of $n = \pm 1$ mode, plotted in Fig. 2.6. Thus, the maximum enhancement is mainly originated from the near field enhancement generated by the azimuthal SP of $n = \pm 1$ order.

Fig. 4.2: Fig/ome0-d.PNG

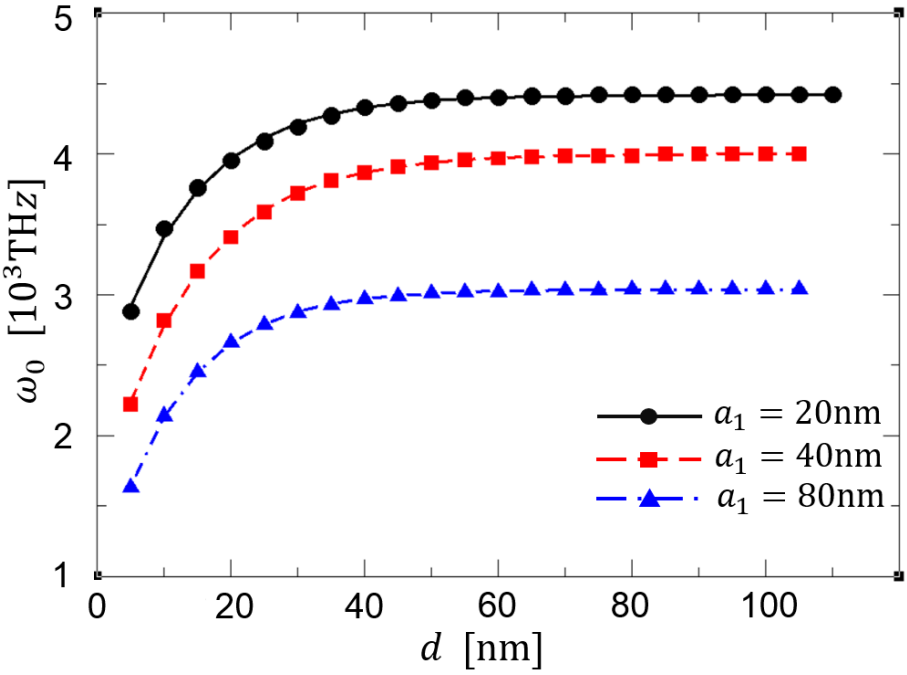

Figure 4.2 ω_0 as a function of d for different a_1. Dots represents the numerical solution calculated from Eqs. (2.130) and (2.131), lines represent the fitting of ω_0 with exponential function given by Eq. (4.3).

By substituting the expressions we get for ω_0, h and γ back in Eq. (4.2), we could then get an approximate expression of enhancement $|\mathbf{E}/E_0|$ as a function of ω, a_1 and d. In Fig. (4.3), we plot the $|\mathbf{E}/E_0|$ we calculated from numerical calculation [calculated from Eqs. (2.130) and (2.131)] and the fitting procedure [Eqs. (4.2) - (4.5)] in a same figure. We can observe from Fig. (4.3), that for a given geometry, the fitting procedure gives an enhancement spectrum close to those calculated from numerical calculation.

Equation (4.1) provides an analytical expression of enhancement as a function of incident frequency ω and geometry parameters a_1 and d. In the next section, we will use the obtained analytical expression for obtaining the optimized geometry that gives the maximum enhancement for a given frequency of incident light.

Fig. 4.3: Fig/peak-compare.PNG
Fig. 4.4: Fig/optimized.PNG

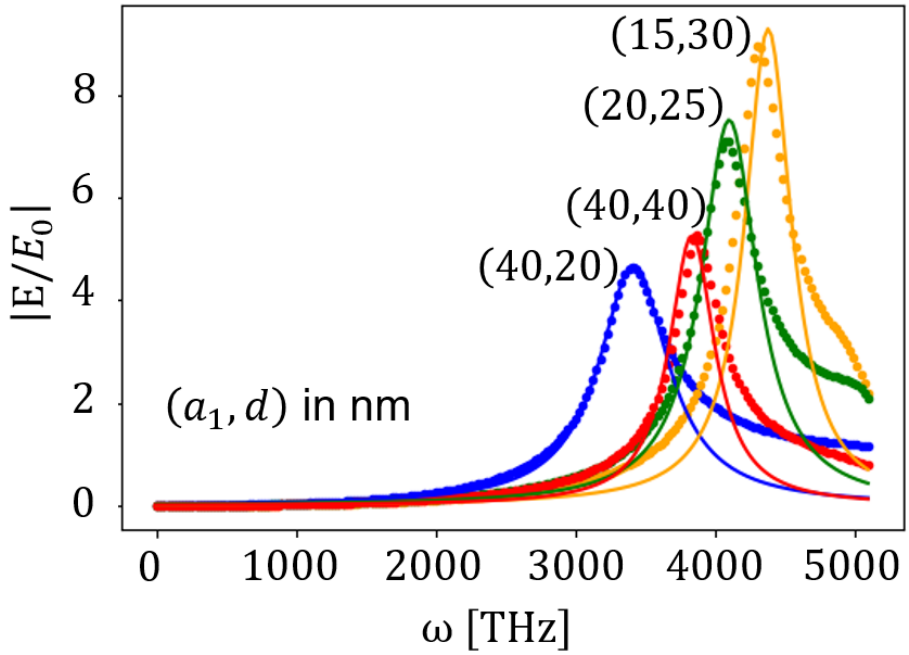

Figure 4.3 $|\mathbf{E}/E_0|$'s from numerical calculation are given by the colored dots for several geometries while that from analytical expression [Eq. (4.2)] are given by solid lines with the same color. The geometries of the spectrum was written in the bracket.

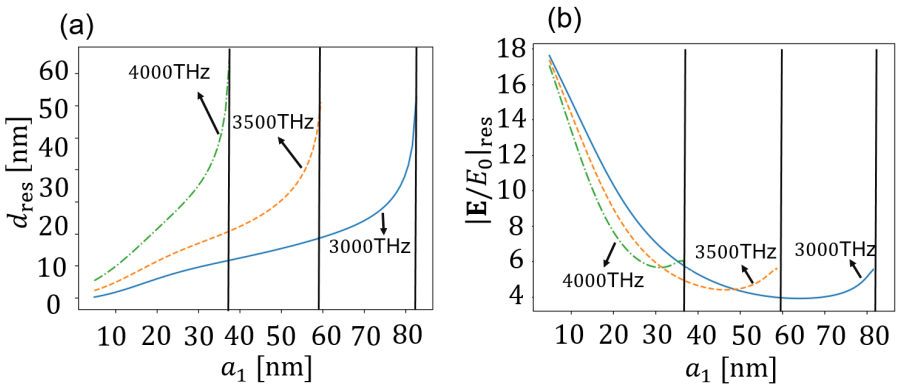

Figure 4.4 (a) Optimized thickness d_{res} and (b) Optimized enhancement $|\mathbf{E}/E_0|_{res}$ plotted as functions of a_1 under given resonance frequencies. Blue solid line for $\omega_0 = 3000$ THz, orange dash line for $\omega_0 = 3500$ THz, green dot dash line for $\omega_0 = 4000$ THz. Vertical lines represent the critical geometries $a_1 = a_1^{\text{crit}}$ of the corresponding spectrum.

4.2 Optimized geometry

In this section we try to find the possible geometry value range for field enhancement peak to exist, and the way to find the optimized geometry if the incident light frequency is given.

Resonant frequency as depicted in Fig. 4.2 decreases as d increase, which means for a given a_1, there would be an upper limit of ω_0. When $d \to \infty$ in Eq. (4.3), we will get the upper limit of frequency $\omega^{[\mathrm{sat}]}$ for a given inner radius a_1:

$$\omega^{[\mathrm{sat}]}(a_1) = 4.84 \times 10^1 - 2.22 \times 10^{-2} a_1. \tag{4.8}$$

$\omega^{[\mathrm{sat}]}$ determines the saturated value of resonance frequency ω_0 as $d \approx \infty$ for a given inner radius a_1, when $\omega_0 > \omega^{[\mathrm{sat}]}$, the peak enhancement caused by azimuthal SP in a cylinder will not occur, no matter what value of the thickness d is.

More importantly, from Eq. (4.8) we can also get the expression of critical geometry $a_1^{[\mathrm{sat}]}$ to get resonance condition for a given incident light frequency ω, which is written as follows:

$$a_1^{[\mathrm{up}]} = 2.18 \times 10^3 - 4.5 \times 10^1 \omega, \tag{4.9}$$

Equation (4.9) determines the upper limit of a_1 for getting the resonance condition for a given incident light frequency ω.

Now we want to present an expression of the optimized parameters. For a given incident light frequency ω, the resonant condition requires $\omega = \omega_0$. By using Eq. (4.3), we can get an expression of optimized d as function of a_1 for any given $\omega = \omega_0$:

$$d_{\mathrm{res}} = \frac{\ln\left(\omega_0 - p_1(a_1)\right) - \ln p_2(a_1)}{p_3(a_1)}. \tag{4.10}$$

By substituting $d = d_{\mathrm{res}}$ into Eq. (4.4), we get the optimized enhancement $|\mathbf{E}/E_0|_{\mathrm{opt}}$ as a function of a_1 for a given ω_0 as follows:

$$|\mathbf{E}/E_0|_{\mathrm{opt}} = \frac{p_4(a_1)}{1 + \left(\frac{\ln\left(\omega_0 - p_1(a_1)\right) - \ln p_2(a_1) - p_3(a_1)p_5(a_1)}{p_3(a_1)p_6(a_1)}\right)^2} + p_7(a_1) e^{-p_8(a_1)\frac{\ln\left(\omega_0 - p_1(a_1)\right) - \ln p_2(a_1)}{p_3(a_1)}}. \tag{4.11}$$

In Fig. 4.4, we plot d_{res} and $|\mathbf{E}/E_0|_{\mathrm{opt}}$ to a_1 for several given ω_0. We find that, in consistence with the result given in Sec. 3.1 the enhancement is generally very large

(more than 14 times) with very small a_1 and d, which coincides the result shown in Fig. 3.3. Another region of significant optimized enhancement is when $a_1 \to a_1^{[\mathrm{up}]}$, $d \approx 60$ nm. Eqs. (4.10) and (4.11) can be used to find the optimized geometry parameters of the metallic hollow cylinder when the incident light frequency is determined.

Chapter 5

Conclusions

In this thesis, we present the study of the electric field enhancement generated by surface electromagnetic (EM) modes in a metallic hollow cylinder. A surface plasmon (SP) mode has a mathematical structure of a surface TM mode. There are two types of surface TM modes on a hollow cylinder, one type propagates along the axis of the cylinder, i.e an axial SP, while another type oscillates around the circumference, i.e. and azimuthal SP. We inspect the case of a cylinder with a dielectric core in vacuum. The axial SP cannot be excited by a light in vacuum, while an azimuthal SP can be excited by shading a light to the cylinder. From the numerical simulation we find that the excited azimuthal SP yields a strong electric field enhancement inside the cylinder. We find that such enhancement is generated mainly by the azimuthal SP mode of $n = \pm 1$ order. Such strong enhancement would enhance light absorption rate inside the cylinder.

We then try to provide analytical relation between radii of the cylinder, incident frequency and the enhancement, so that we can use such mathematical relation to find out the optimized structure to generate strongest near field enhancement inside the cylinder for any incident light with a given frequency, or vise versa. We finds that the enhancement spectrum can be represented as a Lorentzian function as a function of frequency ω, while the parameters of this Lorentzian function determines the optimized enhancement and the resonance frequency. The expression of these parameters of Lorentzian function was fitted as a function of geometry parameters a_1 and d, from which we obtain the critical geometry and critical frequency to generate

azimuthal SP, and then we obtain the optimized geomtery for a given frequency of the incident light.

Appendix A

Calculation Programs

Most of the calculation in this thesis is done analytically. Beside fitting and the plotting, the numerical calculation was mainly used for the calculation of the dispersion and the calculation of the enhancement, in both situations, the major job is the solving of either an 8×8 matrix equation or a 4×4 matrix equations which is the simplified version of the previous equation. The core part of most of the programs we presents here are essentially the same.

All the necessary programs can be found under the following directory in FLEX workstation.

tian/python/cylinder

A.1 Dispersion for axial surface plasmon in hollow cylinder

`Program: hollowaxial.py`

`Inputs:`

Geometry parameters a1 and a2 and index n can be changed.

`Outputs:`

The dispersion relation is plotted and saved as file dispersionaxial.jpg

A.2 Dispersion and the enhancement for azimuthal surface plasmon in hollow cylinder

`Program: nmmodes.py`

`Inputs:`

Geometry parameters a1 and a2 and index n can be changed, The data range ran for 2d spacial plot of the enhancement can be changed to fit the diameter.

`Outputs:`

The dispersion relation is plotted and saved as file dispersionazimuthal.jpg, 2d spacial plot of the enhancement is saved as file '2denhancement.jpg'. The plot of the enhancement along x-axis and y-axis is saved in files 1denhancementx.jpg and 1denhancementy.jpg, repsectively.

A.3 Enhancement spectrum and the fitting

`Program: azimuthalfitting.py`

`Inputs:`

Geometry parameters a1 and d, the fitting range omerange and initial guess of the fitting function.

`Output:`

The parameters w0, gam and g of the Lorentzian fitting function, which will be printed on screen and in output.txt, the numerically calculated spectrum of the enhancement and the enhancement plotted from the fitting Lorentzian function would be printed as file azifit.jpg, with the derivation of the fitting shown on the figure. After every fitting operator should check the accuracy of the fitting, and decide whether to collect the data or discard it.

Presentation list

Oral presentations

1. **Y. Tian**, M. S. Ukhtary, R. Saito: Enhancement of electric field by surface plasmon on hollow cylinder. Presented in ATI 2019 Nano-Carbon Meeting and Zao19 Meeting (2019.8.8-9), Yamagata-Zao, Japan.

Poster Presentations

1. **Y. Tian**, F. R. Pratama, M. S. Ukhtary, R. Saito: The enhancement of the electric field around the metallic cylindrical tube. Presented in 56th Fullerene-Nanotubes-Graphene General Symposium of Nanotubes (2019.3.2-4), Tokyo, Japan.

2. **Y. Tian**, M. S. Ukhtary, R. Saito: Enhancement of electric field by surface plasmon on hollow cylinder. Presented in 57th Fullerene-Nanotubes-Graphene General Symposium of Nanotubes (2019.9.3-5), Nagoya Japan.

Bibliography

[1] F R Pratama, M Shoufie Ukhtary, and Riichiro Saito, Condens. Matter 31 265701 31, 265701 (2019).

[2] Ryan Beams, Journal of Raman Spectroscopy 49(1), 157–167 (2018).

[3] Bruno Pettinger. Tip-enhanced Raman spectroscopy (TERS). In Surface-Enhanced Raman Scattering, pages 217–240, Springer, 2006.

[4] Nicolas Guillot, Hb Shen, B Frémaux, Olivier Péron, Emmanuel Rinnert, Timothée Toury, and M Lamy de la Chapelle, Applied Physics Letters 97(2), 023113 (2010).

[5] F Keilmann, Journal of microscopy 194(2-3), 567–570 (1999).

[6] AE Kryukov, Y-K Kim, and John B Ketterson, Journal of applied physics 82(11), 5411–5415 (1997).

[7] Kristofer Tvingstedt, Nils-Krister Persson, Olle Inganäs, Aliaksandr Rahachou, and Igor V Zozoulenko, Applied Physics Letters 91(11), 113514 (2007).

[8] Kui Bao Ulf H?kanson Naomi J. Halas PeterNordlander Shunping Zhang, Hong Wei and Hongxing Xu, 107(9), 096801 (August 2011).

[9] Dror Sarid and William Challener, Modern introduction to surface plasmons: theory, Mathematica modeling, and applications (Cambridge University Press, Cambridge, 2010).

[10] J. E. Inglesfield, Solid State Communications 40, 467–471 (1981).

[11] Mario Rocca, Surface science reports 22(1-2), 1–71 (1995).

[12] Stefan Alexander Maier, Plasmonics: fundamentals and applications: fundamentals and applications (Springer Science & Business Media, Bath, 2007).

[13] M Shoufie Ukhtary and Riichiro Saito, Carbon (2020).

[14] Anatoly V Zayats and Igor I Smolyaninov, Journal of Optics A: Pure and Applied Optics 5(4), S16 (2003).

[15] VS Zuev, AV Frantsesson, J Gao, and JG Eden, The Journal of chemical physics 122(21), 214726 (2005).

[16] A Yelon, KN Piyakis, and E Sacher, Surface science 569(1-3), 47–55 (2004).

[17] Ellen J. Zeman and George C. Schatz, Journal of Physical Chemistry, 91, 634–643 (1987).

[18] Alexandre Vial, Anne-Sophie Grimault, Demetrio Macías, Dominique Barchiesi, and Marc Lamy de la Chapelle, Physical Review B 71(8) (feb 2005).

[19] Anastasiya Derkachova, Krystyna Kolwas, and Iraida Demchenko, Plasmonics 11, 941–951 (2016).

[20] Alexandre Vial, Anne-Sophie Grimault, Demetrio Macas, Dominique Barchiesi, and Marc Lamy de la Chapelle, Physical Review B 71(8) (feb 2005).

[21] Bo Johnsson, Stefan Löfås, and Gabrielle Lindquist, Analytical biochemistry 198(2), 268–277 (1991).

[22] Eliza Hutter and Janos H Fendler, Advanced materials 16(19), 1685–1706 (2004).

[23] Dajian Wu, Xiaojun Liu, and Bo Li, Journal of Applied Physics 109(8), 083540 (2011).

[24] Barbora Špačková, N Scott Lynn, Jiří Homola, Pavel Kwiecien, and Ivan Richter. In SENSORS, 2012 IEEE, pages 1–4. IEEE, 2012.

[25] D Taverna, M Kociak, V Charbois, and L Henrard, Physical Review B 66(23), 235419 (2002).

[26] DJ Mowbray, S Segui, J Gervasoni, ZL Mišković, and NR Arista, Physical Review B 82(3), 035405 (2010).

[27] Shulin Sun, Hung-Ting Chen, Wei-Jin Zheng, and Guang-Yu Guo, 21, 14591 (2013).

[28] Diego M Solis, Jose Manuel Taboada, Luis Landesa, Jose Luis Rodriguez, and Fernando Obelleiro, Progress In Electromagnetics Research 154, 35–50 (2015).

[29] Harald Ditlbacher, Andreas Hohenau, Dieter Wagner, Uwe Kreibig, Michael Rogers, Ferdinand Hofer, Franz R Aussenegg, and Joachim R Krenn, Physical review letters 95(25), 257403 (2005).

[30] Qian Zhao, Ji Zhou, Fuli Zhang, and Didier Lippens, Materials today 12(12), 60–69 (2009).

[31] R Sainidou and FJ García de Abajo, Optics express 16(7), 4499–4506 (2008).

[32] Ken-ichi Sasaki, Shuichi Murakami, and Hideki Yamamoto, Applied Physics Letters 108(16), 163109 (2016).

[33] Milton Abramowitz, Irene A Stegun, and Robert H Romer. Handbook of mathematical functions with formulas, graphs, and mathematical tables, 1988.

[34] Craig F Bohren and Donald R Huffman, , 2008).

[35] Julius Adams Stratton, Electromagnetic Theory (John Wiley & Sons, Piscataway, 2007).

[36] CA Pfeiffer, EN Economou, and KL Ngai, Physical review B 10(8), 3038 (1974).

[37] Ilja N Bronshtein and Konstantin A Semendyayev, Handbook of mathematics (Springer Science & Business Media, Berlin, 2013).

[38] C Leubner, Physical Review A 23(6), 2877 (1981).

[39] H Hövel, S Fritz, A Hilger, U Kreibig, and Michael Vollmer, Physical Review B 48(24), 18178 (1993).

[40] Kheirandish Asef, Sepehri Javan Nasser, and Mohammadzadeh Hosein, Scientific Reports (Nature Publisher Group) 10(1) (2020).